Traveling Flames on Ring Shaped Troughs

Yanting Song, Yiyi Xu, Kaiyan Yao

Nanjing Foreign Language School, Nanjing 210022, China

E-mail: songyanting0212@gmail.com, xu3712965@gmail.com, kaiyanyao09@gmail.com

Abstract

This study investigates the dynamics of traveling flames of flammable liquid on ring-shaped troughs, using an integrated framework of theory, experiments, and computational simulations. We find that the combustion systems with low-Lewis-number (Le < 1) are mathematically isomorphic to generalized excitable media, exhibiting characteristic behaviors, such as threshold excitation, refractory periods, and wave annihilation, making flame propagate in a circle instead of burning simultaneously. We identify such a phenomenon in experiments and change parameters such as trough diameter from 3 mm to 10 mm, ring diameter from 60 mm to 150 mm, and fuel height from 1.4 mm to 3.0 mm. A theoretical model is developed that successfully predicts the flame velocity by introducing independent efficiency factors for the effects of the trough's width and curvature based on the evaporation combustion balance of the fuel. Furthermore, we utilize two complementary computational approaches—Computational Fluid Dynamics (CFD) and Physics Informed Neural Networks (PINN) to simulate these phenomena. The results of this research provide new insights into the complex dynamics of combustion propagation and offer valuable references for related engineering applications.

Keywords: Flame propagation, excitable media, Lewis number, thermo-diffusive instability, ring combustion, nonlinear dynamics, PINN, CFD

CONTENTS

I	Introdu	action	
II	Experimental Investigation		
	II-Ā	Experimental Design and Apparatus	.
	II-B	Experimental Results	•
	II-C	Experimental Discussion	,
II	Theore	tical Foundation: Combustion as an Excitable Medium	!
	III-A	Boundary Condition for Flame propagation	. 1
	III-B	Lee evaporation-condensation model	. 1
	III-C	From Zeldovich–Frank-Kamenetskii Theory to Flame velocity	. 1
	III-D	Analogy between Combustion and Excitable Media	. 1
	III-E	Geometric Constraints and Influences	. 1
	III-F	Instability of Flame Front	. 2
		III-F1 Darrieus-Landau (DL) Instability	. 2
		III-F1 Darrieus-Landau (DL) Instability	. 2
		III-F3 Quantitative Analysis and Impact on Flame velocity	. 2
		III-F4 Empirical Models for Flame Acceleration	. 2
	III-G	Theoretical Results and Discussions	2
	III O	III-G1 Influences of Ring Diameter	. 2
		III-G2 Influences of Trough Diameter	. 2
		III-G2 Influences of Trough Diameter	. 2
		ini-os innuences of ruci ficigin	
IV	Implen	nented Machine Learning Method for Computational Fluid Dynamics and Therma	al
Dyna		Tomoca Minemine Bearining Meetical Compositional Finances and Finemine	2
	IV-A	PINN Architecture and Implementation	
	IV-B	Computational Fluid Dynamics Algorithm using MATLAB	
	IV-C	Hybrid PINN-CFD Method	
	IV-D	Results and Discussions	. 3
	110	IV-D1 Line shaped	. 3
		IV-D1 Line shaped	. 3
		IV-D3 Ring shaped	_
		TV-D3 King shaped	. 3
V	Future	Prospects	3
VI	Conclu	sions	3
		X . 2 /	
Refe	rences		3
		1, 1, 1, 1, 1, 1, 1, 1, 1, 1, 1, 1, 1, 1	
	6		
	ソく		
こし	/ ^ `		
7	M		
	NT		

I. Introduction

The dynamics of flame propagation in confined geometries is a fundamental challenge in combustion science with critical implications for energy systems, propulsion technologies, and safety engineering [1]. While most fire science research focuses on the macroscopic spread of wildfires across vast landscapes, there is a relative scarcity of research on micro-scale flame dynamics within confined structures. When a thin layer of flammable liquid fills a ring-shaped trough, the resulting flame can continuously propagate around the trough, exhibiting rich dynamical behaviors that transcend classical combustion theory [2]. The study of flame propagation in such a curved geometry is a novel area, as the unique properties of the ring introduce new physical mechanisms that can lead to a self-sustaining, periodic combustion state. This research aims to systematically explore this phenomenon, addressing the central question of how the characteristics of this traveling flame depend on the system's physical and geometric parameters, and whether a unified predictive framework can be developed.

After the phenomenon of ring propagating on a ring shaped trough is observed in experiment, we begin to investigate the underlying mechanism. In the experiment, liquid fuel evaporates into gaseous vapor under the action of heat. Subsequently, driven by turbulence induced by thermal convection in the groove, the vapor fully mixes with air to form a combustible mixture. The heat released by combustion near the ignition source not only ensures the continuity of the reaction but also heats the adjacent unburned mixture to promote flame propagation. The system eventually reaches a dynamic equilibrium: the heat released by the flame exactly meets the latent heat of vaporization required for the fuel to maintain its current evaporation rate, and the fuel evaporation rate perfectly matches the combustion consumption rate, thereby achieving sustained combustion of the flame.

The key reason why the flame rotates along the annular groove instead of burning the entire ring simultaneously lies in the "refractory period" phenomenon observed in the experiment. After the flame passes through a certain region, the fuel in that region is rapidly consumed, and the temperature cannot reach the ignition threshold of the mixture again in a short time. This refractory period turns the burned region into a "non-excited region", forcing the flame to continuously propagate towardss the fresh unburned mixture ahead. Combined with the geometrically closed characteristic of the annular groove, the flame ultimately exhibits a rotational movement along the circumferential direction of the groove rather than synchronous combustion of the entire ring. Therefore, we adopt a comprehensive framework of Lee

evaporation model, ZFK theory and excitable medium that integrates theoretical analysis by making an analogy between combustion systems and excitable media. This innovative perspective allows us to better understand characteristic flame behaviors such as threshold excitation, refractory periods, and wave annihilation, providing a new theoretical foundation for explaining why flames can form self-sustaining periodic movements within a ring.

For our further analysis, we utilized two cutting-edge computational tools: Computational Fluid Dynamics (CFD) and Physics-Informed Neural Networks (PINN). CFD has a long and established history as a powerful tool in the fields of fluid mechanics and heat transfer, capable of providing high-fidelity modeling for complex physical processes. On the other hand, PINN is an emerging deep learning framework that solves partial differential equations by embedding physical laws directly into the loss function of the neural network. This method shows great potential for solving both forward and inverse problems involving nonlinear partial differential equations. The core innovation of this study lies in the organic fusion of these two methods. Our developed hybrid algorithm, operating within a MATLAB environment, combines the precision of CFD in fluid dynamics and thermodynamics with the flexibility of PINNs in handling complex nonlinear equations. This integrated model is capable of more accurately simulating fuel consumption, flame front evolution, and temperature field distribution. The resulting simulations are more closely aligned with the experimental observations than those obtained from a single model.

This research makes key contributions to the fields of fire dynamics and computational science by providing a novel theoretical framework—treating the combustion system as an excitable medium for the first time, along with a proof of its isomorphism—which offers a fresh perspective for understanding flame dynamics. Furthermore, we successfully developed a novel PINN-CFD fusion algorithm and effectively applied it to simulate flames in a circular trough. To our knowledge, only one recent paper has explored the general concept of a PINN-CFD fusion model [3]. Our work is the first to apply this method to a specific combustion problem, and demonstrate its superiority in simulating flame propagation.

This innovative theoretical framework and computational method provide a powerful new tool for fire science. They not only enable more accurate predictions of flame behavior in specific geometric structures but also lay the foundation for future research on flame dynamics in more complex environments, such as urban or confined-space fires.

II. EXPERIMENTAL INVESTIGATION

In the introduction, we mentioned and described the phenomenon of the problem. In order to get a clearer physical image of the problem, we first made an experimental phenomenon and tried to analyze and draw conclusions from the phenomenon.

A. Experimental Design and Apparatus

To demonstrate the phenomenon, we prepared using a custom-designed, 3D printed aluminum alloy ring, an electronic lighter for ignition, and a micropipette for precise fuel dispensing. The fuel consisted of a mixture of Zippo oil vapor and air. Then, we used a tripod and a camera (Sigma FP) to take the shots shown in Figure 1. Specifically, our experimental setup employs custom-designed, 3D-printed aluminum alloy rings manufactured using Fusion 360 CAD software. The baseline configuration features a ring diameter of 150 mm with a semicircular trough of 10 mm diameter. From this reference design, we performed parametric studies by varying the diameter of the ring from 50 mm to 150 mm in increments of 10 mm (11 configurations), the trough diameter from 3 to 10 mm in increments of 1 mm (8 configurations) and the orientation of the trough of the inward, outward, and five special geometries (7 configurations). This systematic variation enables the isolation of the effects of individual parameters on the characteristics of flame propagation shown in Figure 2.

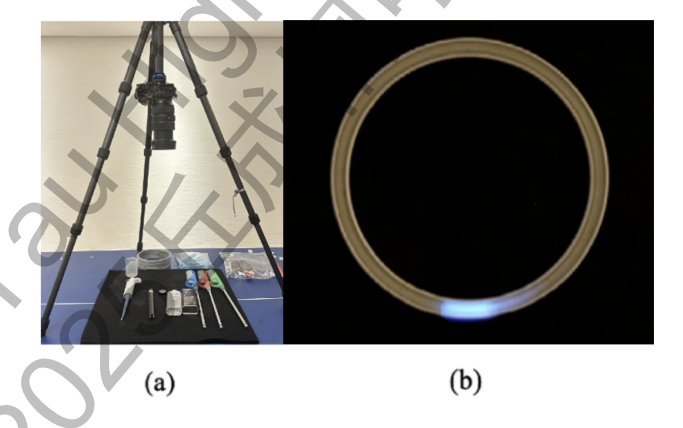


Fig. 1: (a) Experimental apparatus showing the 3D-printed aluminum ring, a beaker, an electronic lighter, a micropipette, a camera, and a tripoda; (b) A detailed ring model with traveling flame.

Before conducting the experiment, we fixed the camera on a tripod, ensuring that the plane of the camera lens was level with the desktop and that there were no other light sources in the entire experimental environment. After setting up the basic conditions, we first poured the fuel into a beaker, then adjusted the

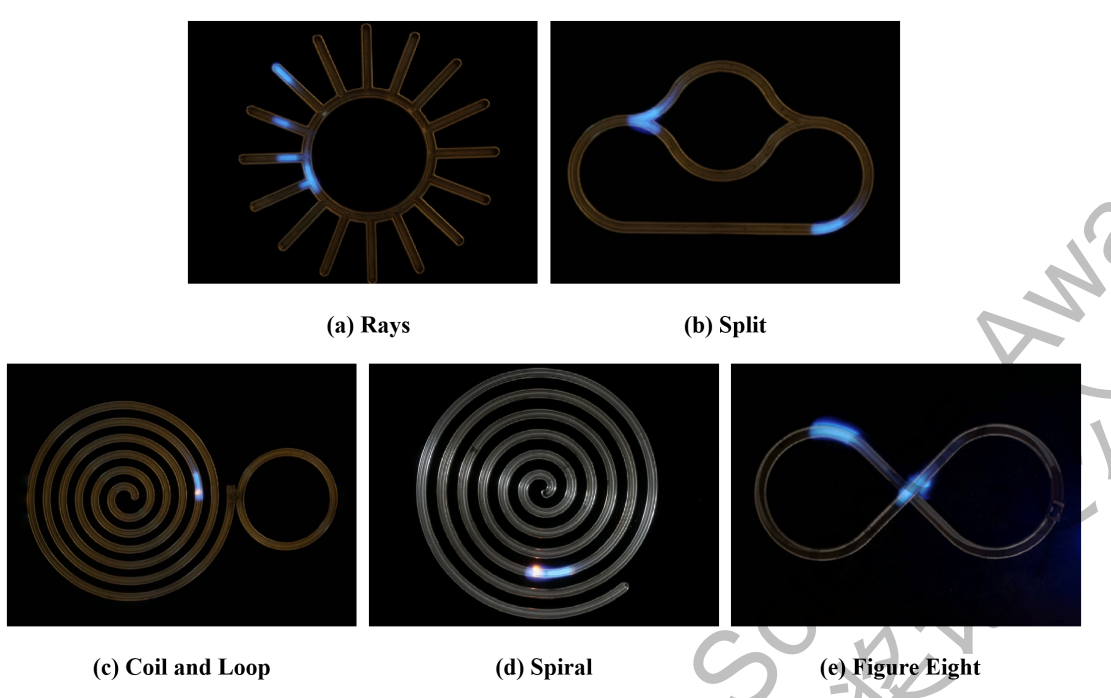


Fig. 2: (a) Rays, (b) Split, (c) Coil and Loop, (d) Spiral, (e) Figure Eight.

pipette so that it could aspirate a specific volume of Zippo oil each time (different volumes as needed). Next, we used the pipette to take the fuel and slowly added it into the troughs of different models placed on the fire blanket. We then started recording with the camera, ignited the fuel in the troughs using an electronic igniter, and paused the recording after the flame had completely extinguished. We conducted the experiment 10 times for each model to ensure at least one successful trial.

After obtaining the experimental videos, we used Tracker software to analyze the successful experimental phenomena (i.e., the flame continuously rotated as a single unit for more than two cycles in the aluminum alloy ring, with a duration exceeding 2 seconds, which corresponds to more than 48 data points). When tracking the flame, we generally focused on its leading edge. A typical successful experiment could yield approximately 50 to 500 consecutive data points. We calculated the flame's velocity and angular velocity by applying the error propagation function to the data points obtained from the experiments, and summarized the flame characteristics under different parameters with error bars. After acquiring accurate data, we calculated the degree of matching between the data points and the theory, and conducted various simulations based on this to study the flame's characteristics.

In our parameter survey, we found that the experimental phenomena are related to several parameters such as the ring diameter, trough diameter, and fuel height. The first two parameters have been realized

by 3D-printing aluminum alloy rings with appropriate parameters, while the third variable cannot be directly measured by simple means due to the special geometric structure of the annular track. Therefore, we introduce Equation 1 to approximately and progressively derive the relative height of the fuel by measuring some simple physical quantities, thereby controlling the variables for further research.

$$S = r^2 \arccos\left(1 - \frac{h}{r}\right) - (r - h)\sqrt{h(2r - h)} = \frac{V}{2\pi R}.$$
 (1)

We can derive the expression for the fuel area by combining Equation 1. Since this is a transcendental equation involving an arccosine function and a radical term, it is impossible to derive an explicit expression for the height through elementary algebra. However, even though we cannot obtain a general solution for the height in a simple form, we can still substitute specific experimental values to find the approximate height under particular cases. Then we can obtain useful regulations through parameter investigations.

B. Experimental Results

After we successfully replicated the traveling flame phenomenon in our experiments, where a small flame propagates around a ring, we change different parameters to investigate how these factors affect the flame speed, specially fuel height from 1.4 mm to 3.0 mm, trough diameter from 3 mm to 10 mm, and ring diameter from 50 mm to 150 mm.

Figure 3 shows how the velocity of the flame changes with the height of the fuel in various diameters of the troughs. The data indicates a clear trend: as the trough diameter increases from 3 mm to 10 mm, the average flame velocity generally increases. The velocity of the flame also fluctuates with changes in the height of the fuel, suggesting that other factors, such as the physical state of the fuel or the variation in the local mixture, also influence the behavior of the flame.

Figure 4 details the effect of ring diameter on flame velocity. When the ring diameter is small, specifically from 6 cm to 8 cm, the flame's angular velocity is at its highest, and the data shows significant fluctuations. This suggests that the flame propagation is fast but unstable in this configuration. As the ring diameter increases to between 9 cm and 13 cm, the flame velocity decreases markedly, and the fluctuations become less pronounced, indicating a more stable propagation. Finally, for the largest diameters (14 cm and 15 cm), the angular velocity reaches its lowest values, showing that the flame propagates much more slowly in these larger rings.

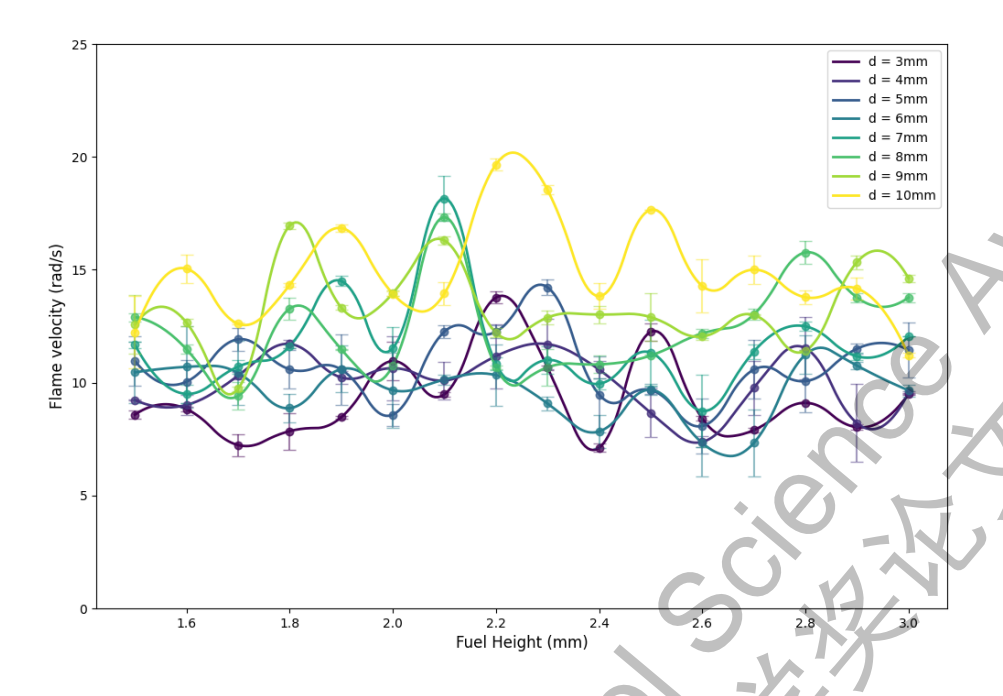


Fig. 3: Relationship between the fuel height and the flame's angular velocity in 8 cases with different trough diameters.

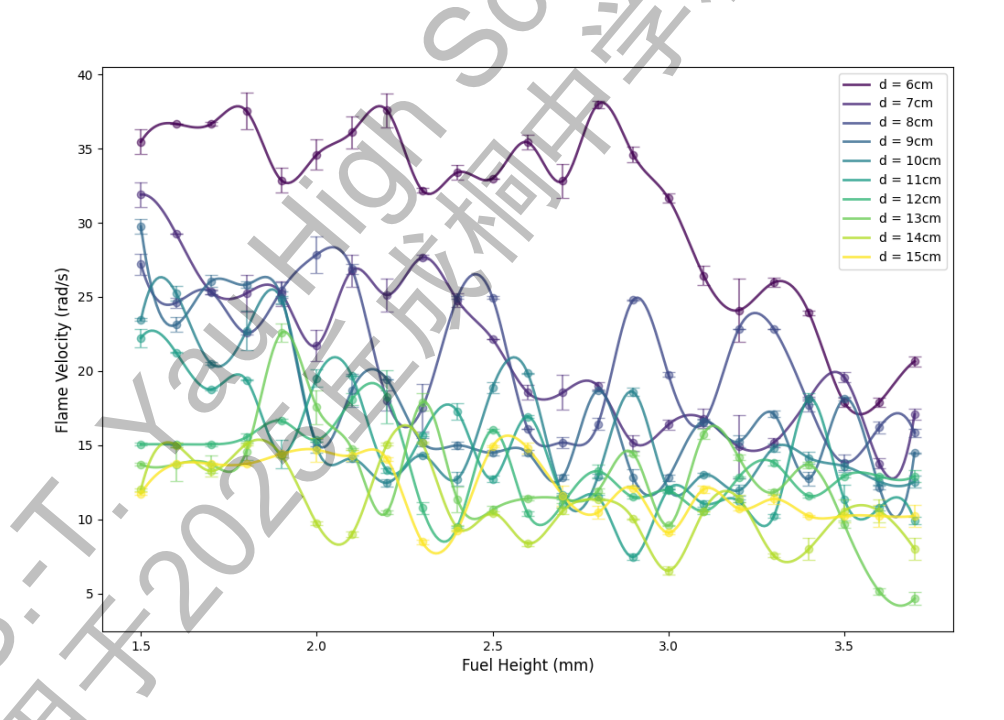


Fig. 4: Relationship between the fuel height and the flame's angular velocity in 10 cases with different ring diameters.

C. Experimental Discussion

The key reason the flame rotates along the annular trough instead of consuming the entire ring at once is the "refractory period" phenomenon. After the flame front passes through a region, the fuel there is quickly consumed, and high-temperature exhaust gases form a thermal barrier. Additionally, some heat is dissipated through the aluminum trough walls. As a result, the temperature in this region cannot reach the ignition threshold again in a short time, preventing re-ignition.

This refractory period essentially turns the burned region into a "non-excitable region," forcing the flame to continuously propagate toward the fresh, unburned mixture ahead. When combined with the closed geometry of the ring-shaped trough, this mechanism compels the flame to rotate along the circumference rather than to undergo a complete synchronous combustion of the ring. Such explanation can be justified by the phenomenon we observed in experiment, when two flames begin to propagate around the ring and collides, they would disappear, which means the flame will not propagate on the "non-excitable region" as shown in Figure 5.

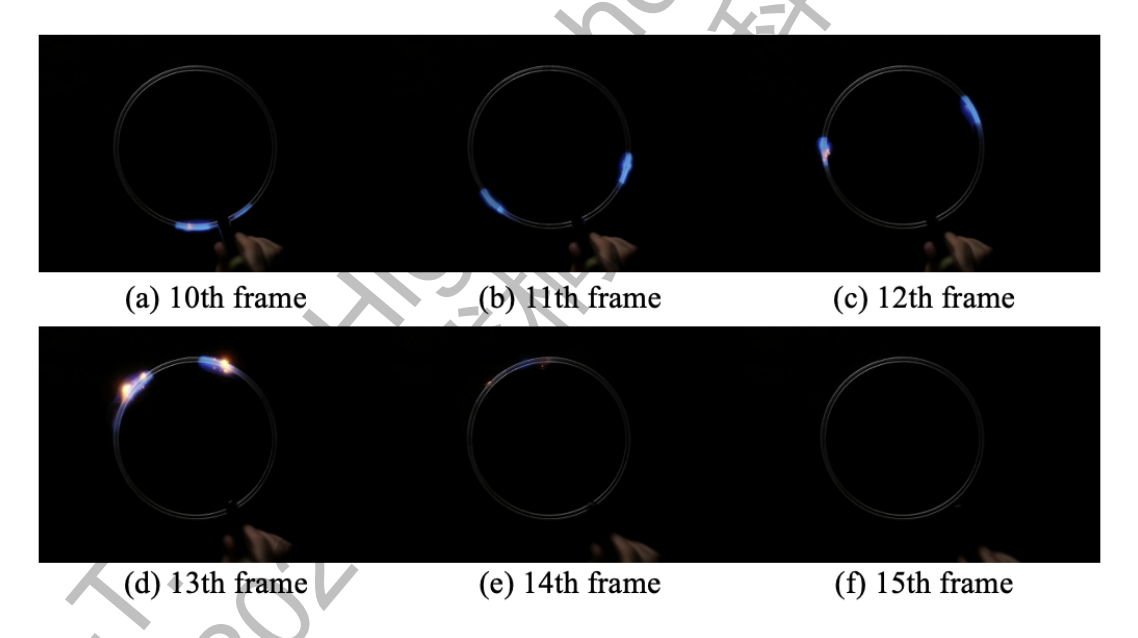


Fig. 5: Two flames propagate and collide.

The stable, rotational combustion of the flame observed in our experiments can be qualitatively explained by the synergistic effects of fuel conversion, mixture formation, and thermal feedback. The ignition source and the heat from combustion cause the liquid fuel to evaporate into a gaseous vapor. This vapor then thoroughly mixes with air, driven by turbulence from thermal convection within the

trough, to form a flammable mixture with the appropriate ratio. Once the initial mixture is ignited, the combustion process releases heat that serves two crucial purposes: it maintains the high temperature of the reaction zone, ensuring the reaction's continuity, and it preheats the adjacent unburned mixture, igniting it and promoting flame propagation. The system eventually reaches a dynamic equilibrium under fixed experimental parameters (e.g., ventilation and fuel pool area). In this state, the heat released by the flame precisely matches the latent heat of vaporization needed to maintain the fuel's evaporation rate, and the fuel evaporation rate is perfectly balanced with the combustion consumption rate. This balance allows for the continuous, self-sustaining combustion of the flame.

As fuel height increases, the flame's angular velocity tends to decrease. This counterintuitive trend can be explained by several factors like thermal barrier, fuel-rich mixture and heat dissipation. For thermal barrier, a thicker fuel layer requires more energy to evaporate. The initial heat from the flame front is less efficient at heating and vaporizing the deeper liquid, creating a "thermal barrier" that slows down the propagation. For fuel-air mixture, with a greater volume of fuel evaporating, the vapor-to-air ratio in the trough might become too high, leading to a fuel-rich mixture. Such a mixture burns less efficiently and more slowly than a stoichiometric (ideal) one, thereby reducing the flame speed. As for heat dissipation, a larger fuel mass acts as a heat sink. The greater volume of liquid can absorb more heat, leading to increased heat loss from the system and a slower overall combustion process.

As the trough diameter increases, the flame velocity generally rises. This is primarily due to two factors. First, a wider trough provides a larger surface area for fuel evaporation and more space for thermal convection. This enhanced mixing leads to a more efficient and uniform vapor-air mixture, which is more combustible and propagates faster. Second, a wider trough mitigates wall effects. In narrow troughs, the proximity of the solid walls causes greater heat dissipation and a quenching effect on the flame, which slows it down. By reducing these interactions, a wider trough allows the flame to propagate more freely and at a higher velocity. The relationship between flame velocity and ring diameter, however, is more complex, revealing a clear dependence on the ring's curvature. When the ring diameter is small, the curvature is high, causing the flame's angular velocity to be at its peak but also highly unstable. The tight bend of the flame front can enhance its speed but also leads to strong thermal and fluid dynamic feedback, resulting in significant velocity fluctuations.

As the ring diameter increases to an intermediate range, the curvature decreases. This allows the

flame to propagate more stably, causing a noticeable reduction in velocity fluctuations and a decrease in speed as the geometric "focusing" effect of high curvature is reduced. For the largest ring diameters, the curvature is minimal. The flame front behaves more like a linear flame, which generally propagates slower than a curved one. In this case, the larger circumference also means the flame must travel a greater distance, contributing to a lower overall angular velocity. As for the fluctuation in the experimental data may be caused by uneven distribution of the fuel, which can be minimized by repetition of experiment by 50 times.

To conclude, the rotating flame phenomenon is primarily due to a "refractory period", where the burned fuel region becomes a non-excitable area that prevents immediate re-ignition. This forces the flame to continuously propagate into fresh fuel, leading to a stable, rotational motion. This can be seen when two flames collide and extinguish each other. The system maintains a stable, self-sustaining combustion as heat from the flame evaporates the fuel, which then mixes with air to form a combustible vapor, and the heat released by this combustion ensures the process continues. The flame's velocity is influenced by several factors. As fuel height increases, the velocity decreases because a thicker layer acts as a thermal barrier, creating a less efficient, fuel-rich mixture and increasing heat loss. Conversely, a wider trough generally increases flame velocity by providing more space for fuel evaporation and mitigating wall effects that would otherwise slow the flame down. The trough's curvature also plays a role: a small diameter (high curvature) leads to high, but unstable, velocities, while a larger diameter (low curvature) results in slower, more stable propagation as the "focusing" effect of high curvature diminishes.

III. THEORETICAL FOUNDATION: COMBUSTION AS AN EXCITABLE MEDIUM

We know that liquid fuel is converted into gaseous fuel molecules (vapor) through different ways like atomization and heating. The fuel vapor then mixes thoroughly and evenly with air (which provides oxygen) under the influence of turbulence, forming a combustible mixture with the right proportions. An ignition source (heat) provides the initial energy to ignite the local mixture. The heat released from this combustion then heats and ignites the neighboring mixture, allowing the flame to propagate. At the same time, the released heat continuously maintains the high temperature of the reaction zone, sustaining the combustion process. Under specific combustion conditions (such as fixed ventilation and fuel pool area), the system reaches a dynamic equilibrium or steady state. In this state, the heat released by the flame

precisely equals the heat required to maintain the current evaporation rate (primarily to provide the latent heat of vaporization), and the evaporation rate is equal to the burning rate.

This section establishes the fundamental theoretical framework that transforms our understanding of flame propagation from a purely thermochemical phenomenon to a manifestation of universal excitable medium behavior. We demonstrate why flames can travel continuously in ring-shaped troughs and derive quantitative predictions for their propagation characteristics.

A. Boundary Condition for Flame propagation

The ability of a flame to propagate continuously around a ring emerges from a delicate balance between competing physical processes [4]. In traditional combustion theory, flame propagation requires a continuous fuel supply and heat transfer. In this study, the phenomenon occurs in the gas-phase region above the liquid surface. The flame itself burns in the gas, causing the liquid fuel below to evaporate through heat transfer. The evaporated fuel vapor then mixes with the air and is reignited by the flame. This cycle continues to propagate forward. Thus, we utilize low-Lewis-number systems to create their own self-sustaining mechanism through thermo-diffusive imbalance.

The Lewis number emerges as the fundamental control parameter determining whether a combustion system exhibits excitable behavior [5]:

$$Le = \frac{\alpha_{th}}{D_m} = \frac{\lambda}{\rho c_p D_m}. (2)$$

where α_{th} is the thermal diffusivity of the mixture of Zippo oil vapor and air, mostly hydrotreated light petroleum distillate, whose specific value depends on temperature and pressure, while under room temperature and atmosphere pressure, the value is around $0.64 \times 10^{-7} \text{ m}^2 \cdot \text{s}^{-1}$ to $0.99 \times 10^{-7} \text{ m}^2 \cdot \text{s}^{-1}$ [6]. D_m is the mass diffusion rate of the vapor molecules of Zippo oil in the surrounding air (mainly nitrogen and oxygen) as a medium. The value of D_m is usually $5.6 \times 10^{-7} \text{ m}^2 \cdot \text{s}^{-1}$ [7].

In conclusion, the greater the α_{th} , the faster the heat travels, and the fuel and air in front of the flame can be heated to the ignition point more quickly. The larger the D_m , the faster the fuel vapor can mix with the air, providing sufficient fuel for the continuous combustion and spread of the flame.

When Le < 1, the system exhibits excitable characteristics because the system has fast thermal diffusion (α_{th} large) that enables rapid heat spread, activating adjacent regions, to be more specific.

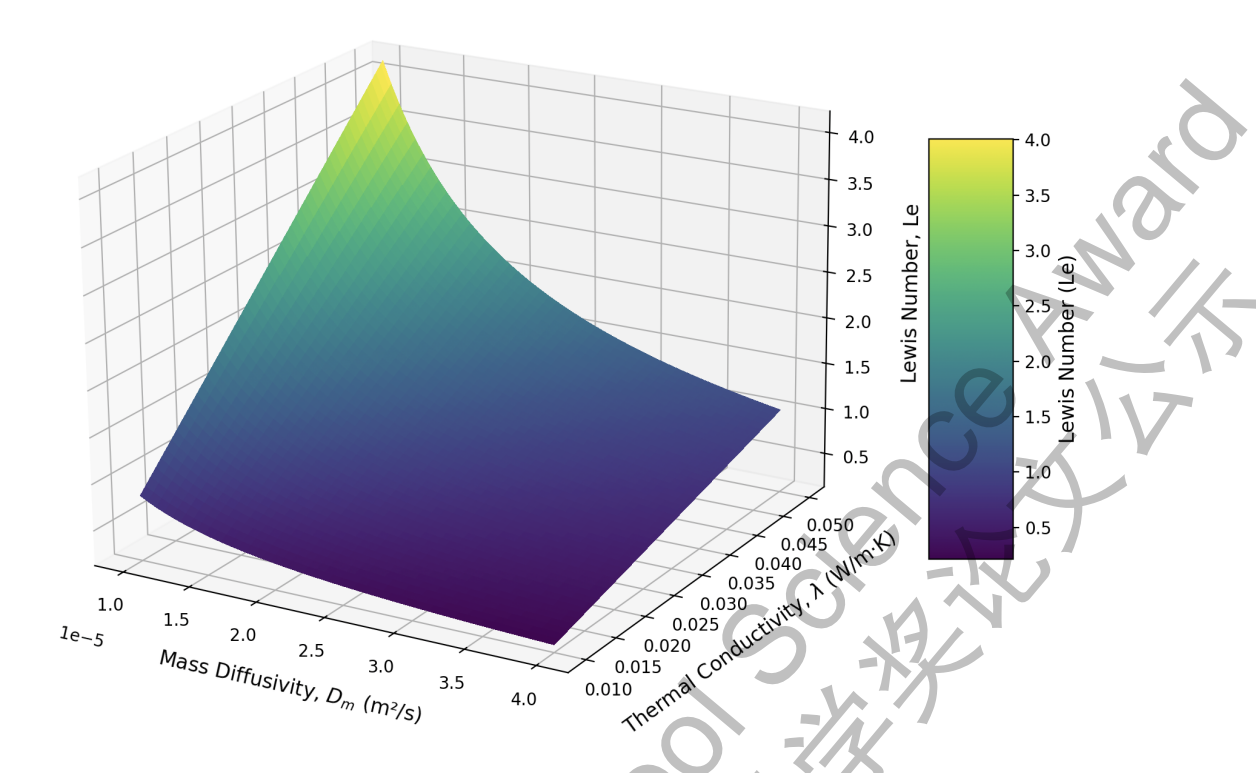


Fig. 6: Phase diagram showing the dependence of the Lewis number on thermal conductivity and mass diffusivity.

The system has a slow mass diffusion (D_m small) that prevents immediate fuel replenishment, creating refractory zones, meaning the part where the flame has "traveled" will not be ignited again in a short period of time. Lastly, the whole system displays thermo-diffusive instability that amplifies perturbations, sustaining wave propagation as observed in experiment. Therefore, the boundary condition for the flame to propagate around a thin trough is demonstrated in Figure 6.

B. Lee evaporation-condensation model

By paralleling "traveling flame" behavior to excitable medium and utilizing Lewis number to give a rough range of the boundary condition for traveling flame and drew a semi-quantitative explanation for this phenomenon, we still need a more accurate theoretical model to accurately explain the physical process and quantify flame combustion and propagation.

The Lee evaporation-condensation model, a simplified yet effective phase-change model, is widely used in computational fluid dynamics to simulate the mass and heat transfer between liquid and vapor phases. Its core principle is that the rate of phase change is directly proportional to the degree of superheating or subcooling at the interface. The model assumes evaporation occurs when the liquid

temperature, T_L , exceeds the saturation temperature, T_{sat} , and condensation occurs when the vapor temperature, T_V , falls below T_{sat} . The mass transfer rate from liquid to vapor, \dot{m}_{evap} , is governed by the linear kinetic equation:

$$\dot{m}_{\rm evap} = c_{\rm evap} \alpha_L \rho_L \frac{T_L - T_{\rm sat}}{T_{\rm sat}} \quad \text{if } T_L > T_{\rm sat}.$$
 (3)

where c_{evap} is an empirical mass transfer coefficient for evaporation, and α_L and ρ_L are the volume fraction and density of the liquid phase. These equations are typically formulated as source terms in a multiphase flow solver's continuity and energy equations. The coefficients c_{evap} and c_{cond} are critical parameters that must be calibrated based on experimental data or higher-fidelity models. These coefficients represent the specific kinetics of the phase change process for a given fluid and system configuration.

C. From Zeldovich-Frank-Kamenetskii Theory to Flame velocity

Lee's theory explains the fuel supply mechanism, which is an important idea to simplify the flame velocity of the ZFK theory using asymptotic analysis using the analogy of "supply and demand" for heat. For flame propagation in a thin, one-dimensional ring geometry, the Zeldovich–Frank-Kamenetskii (ZFK) equation describes the balance between heat diffusion and chemical reaction [8]. The governing equation in its non-dimensional form is:

$$\frac{\partial \theta}{\partial t} = \frac{\partial^2 \theta}{\partial x^2} + \omega(\theta). \tag{4}$$

This equation models the evolution of the non-dimensional temperature, θ , over time, t, and along the spatial coordinate of the ring, x. Note that $\theta(x,t)$ is the non-dimensional temperature with no explicit relationship to T. It is scaled such that $\theta=0$ represents the cold, unburnt liquid and vapor mixture, and $\theta=1$ represents the hot, fully burned products, while x and t are the nondimensional space and time coordinates. $\omega(\theta)$ here is the non-dimensional reaction rate, capturing the highly non-linear nature of combustion chemistry. For high activation-energy reactions, it is typically expressed as:

$$\omega(\theta) = \frac{\beta^2}{2} (1 - \theta) e^{-\beta(1 - \theta)}.$$
 (5)

where β is the Zeldovich number [9]. It is a crucial dimensionless parameter representing the activation

energy of the reaction, which can be represented by

$$\beta = \frac{E_a(T_b - T_u)}{RT_b^2}.$$
(6)

where E_a is the activation energy, the minimum energy required to start combustion rate, T_b is the temperature of the burned gas, which is the final temperature of the gas after combustion, also known as the temperature of the adiabatic flame. T_u is initial temperature of the fuel / oxidizer mixture before burning. R is the universal gas constant. In our case, when the flame is immediately ignited by electronic lighter on petroleum distillate, shown in experiment part, under room temperature and normal atmosphere pressure, E_a is around $126,000~\mathrm{J}\cdot\mathrm{mol}^{-1}$, T_b is $2200~\mathrm{K}$, T_u is $300~\mathrm{K}$ and R is $8.314~\mathrm{J}\cdot\mathrm{mol}^{-1}\cdot\mathrm{K}^{-1}$. Thus, we can calculate $\beta=5.95$. Such result signifies that the chemical reaction is extremely sensitive to temperature and is only significant in a very thin region near the flame front where the temperature is high.

Note that to adapt the ZFK theory to our problem when the flame propagate in a ring shaped trough, we adapt this equation by specify boundary conditions.

$$\theta(0,t) = \theta(L,t)$$
 and $\frac{\partial \theta}{\partial x}(0,t) = \frac{\partial \theta}{\partial x}(L,t)$. (7)

where L represents the total length of the container, including its boundaries. These conditions ensure that the temperature and heat flux are continuous as the flame propagates around the ring and returns to its starting point.

After we have acquired the average reaction rate of combustion of system, we utilize a fundamental property to derive the laminar flame velocity (s_L) of flame, the velocity at which a planar flame front propagates into a quiescent premixed gas:

$$s_L^2 = \frac{2}{\rho_u^2 c_p^2} \int_{T_u}^{T_b} \lambda \dot{\omega} \, dT. \tag{8}$$

Here, ρ_u is the density of the unburned gas mixture, c_p is the specific heat capacity at constant pressure, $\dot{\omega}$ is the chemical reaction rate, T_u and T_b are the temperatures of the unburned and burned gas, respectively [8].

The key to the problem is how to evaluate the integral term in the formula above whereas the essence of the ZFK theory lies in using the high activation energy assumption, namely asymptotic analysis to find an approximate solution for this integral [10]. The reason we can utilize this method is for a reaction rate of the Arrhenius form $\dot{\omega} \propto -\frac{e_a}{RT}$, where E_a the activation energy is very large, the chemical reaction is primarily confined to a very narrow region where the temperature is close to T_b .

Note that asymptotic analysis doesn't solve the full, complicated equation head-on. Instead, it uses a "divide and conquer" strategy to calculate the heat demand and supply separately and then finds the flame velocity s_L that perfectly balances the two. To be more specific, the process of asymptotic analysis can be understood using "supply and demand" analogy for heat. For a flame to propagate steadily, the heat generated by the chemical reaction must be exactly enough to preheat the cold fuel-air mixture ahead of it. Asymptotic analysis translates this physical picture into a solvable mathematical problem in three steps.

We analyzed the preheat zone, also known as the "heat demand". The task is to calculate how much heat is needed to bring the cold, unburnt gas up to its ignition temperature through convection. By looking only at the preheat zone. Here, we ignore the chemistry reaction term since the temperature is still too low for any significant chemical reaction to occur. With this simplification, the heat demand equation is:

$$\dot{q}'_{\text{demand}} = \rho_u s_L c_p (T_{ig} - T_u). \tag{9}$$

where ρ_u is the density of the unburnt gas, here it's equal to $1.2 \text{ kg} \cdot \text{m}^{-3}.c_p$ is the specific heat at constant pressure, which is $1200 \text{ J} \cdot \text{kg}^{-1} \cdot \text{K}^{-1}$. T_{ig} is the ignition temperature, and T_u is the initial temperature of the unburnt gas. This simplified equation can be solved easily to find the temperature profile across the preheat zone.

Then we analyze the reaction zone, also known as "Heat Supply", where we need to calculate how much heat the thin reaction layer can actually generate and supply to the preheat zone. We now focus only on the extremely thin reaction zone where the chemistry happens, by using the key assumption of high activation energy, we can use a clever mathematical integration technique to calculate the total rate of heat generation across this entire layer.

$$\dot{q}'_{supply} = \int_{\text{reaction zone}} \dot{\omega}_T dx. \tag{10}$$

$$\dot{\omega}_T = Q\dot{\omega}_{\text{fuel}} = Q\left(\rho^2 Y_F Y_O B \exp\left(-\frac{E_a}{RT}\right)\right). \tag{11}$$

Q is the heat of reaction per unit mass of fuel. Y_F and Y_O are the mass fractions of fuel and oxidizer, respectively. B is the pre-exponential factor, which is 10^{10} s⁻¹. E_a is the activation energy. R is the universal gas constant, which is 8.314 J \cdot kg⁻¹ \cdot K⁻¹.

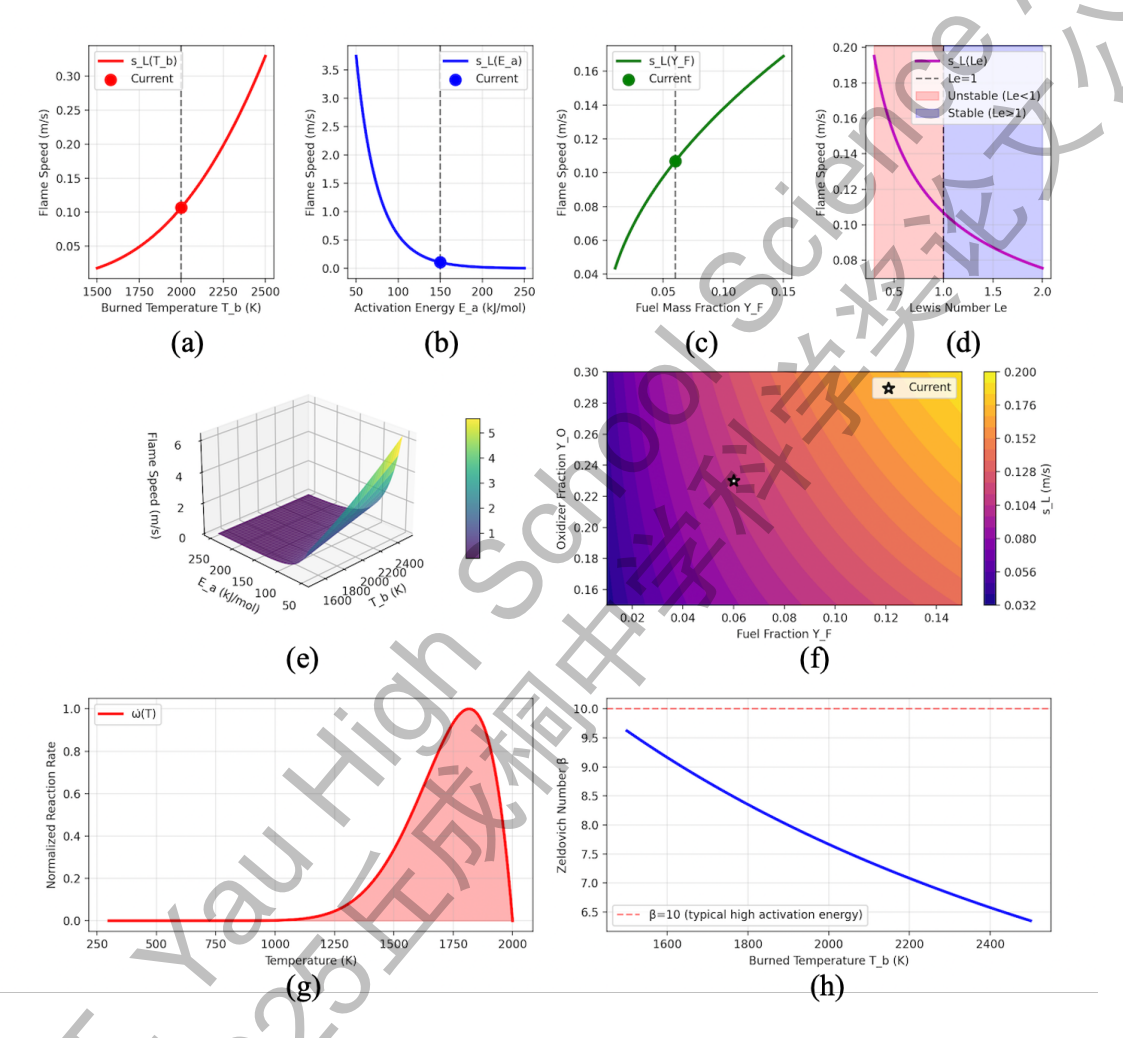


Fig. 7: The direct effects of combustion temperature, activation energy, fuel concentration, and Lewis number on laminar flame velocity, as well as flame velocity surface, reaction rate distribution, and Zeldovich number.

For the flame to be stable, heat demand must be equal to heat supply, which can be written as the equation:

$$s_L^2 \approx 2 \frac{\lambda_b}{\rho_u^2 c_p^2} \left[\rho_b^2 Y_{F,u} Y_{O,u} B \exp\left(-\frac{E_a}{RT_b}\right) \right] \left(\frac{RT_b^2}{E_a}\right).$$
 (12)

Here, the subscripts b and u denote properties in the burnt T_b and unburnt T_u regions respectively, $Y_{F,u}$ and $Y_{O,u}$ are the mass fractions of the fuel and oxidizer in the unburnt region, B is the pre-exponential factor. The relationship between different parameters and flame velocity is shown in Figure 7. The top row of the plots shows the direct impact of the most important parameters. We can see that the laminar flame velocity increases with higher burned temperatures T_b but decreases with a higher activation energy E_a , which represents a larger potential barrier for the chemical reaction to overcome. The plot on the right shows how flame velocity changes with the fuel concentration Y_F , peaking near an optimal fuel-air ratio. The middle row visualizes more complex interactions. The 3D Flame velocity Surface shows the combined influence of temperature and activation energy at a glance. The Lewis Number Effect plot is crucial, as it highlights how the balance between heat and mass diffusion affects the flame. It shows that flames can become unstable when Le is less than one, a critical concept in combustion dynamics. The bottom row reveals the physics behind the calculations and provides a practical guide. The Reaction Rate Profile shows the sharp spike in reaction intensity near the final flame temperature, a core assumption of the model. The plot next to it shows the Zeldovich Number β , a key measure of the reaction's temperature sensitivity. Finally, the Flame velocity Map acts as a performance guide, showing how the flame velocity changes across a range of fuel and oxidizer mixtures, with the star marking a specific operating point. Through ZFK theory, we can calculate the theoretical flame velocity with respect to the position of the flame.

D. Analogy between Combustion and Excitable Media

To justify the parallel between traveling flame phenomena and excitable media, we demonstrate a strong analogy between the Zeldovich-Frank-Kamenetskii (ZFK) theory of combustion and the general theory of excitable media. At its core, this analogy is evident in the simplest forms of both theories. Each is a classic reaction-diffusion system where a state variable is balanced by spatial diffusion and a highly non-linear local reaction. The ZFK equation for temperature (θ) balances heat diffusion with a temperature-sensitive reaction term $F(\theta)$:

$$\frac{\partial \theta}{\partial t} = D \frac{\partial^2 \theta}{\partial x^2} + F(\theta). \tag{13}$$

Here, $F(\theta)$ is negligible at the cold (rest) state and sharply peaked at a high ignition temperature, driving the system to a hot (excited) state. A simple model for an excitable medium's activation variable (v) is structurally similar, balancing diffusion with a non-linear kinetic term G(v):

$$\frac{\partial v}{\partial t} = D \frac{\partial^2 v}{\partial x^2} + G(v). \tag{14}$$

Here, G(v) has stable roots for the rest and excited states, separated by an unstable threshold, representing the system's rapid change.

This fundamental parallel in the single-variable case—a propagating wave driven by diffusion and a threshold-based non-linear reaction-motivates a more rigorous, two-variable analysis. We now formalize this analogy using the more complete two-variable models for combustion (activator-inhibitor) and excitable media. The ZFK theory for a non-adiabatic flame is governed by a system of reactiondiffusion equations for temperature (T) and reactant mass fraction (Y):

$$\frac{\partial T}{\partial t} = \nabla^2 T + \Omega(T, Y). \tag{15}$$

$$\frac{\partial Y}{\partial t} = \frac{1}{Le} \nabla^2 Y - \Omega(T, Y). \tag{16}$$

where T is the activator (temperature), Y is the inhibitor (fuel), Le is the Lewis number, and Ω is the reaction rate. A general excitable medium is described by the FitzHugh-Nagumo type system for an activator (u) and an inhibitor (v):

$$\frac{\partial T}{\partial t} = \nabla^2 T + \Omega(T, Y). \tag{17}$$

$$\frac{\partial T}{\partial t} = \nabla^2 T + \Omega(T, Y). \tag{17}$$

$$\frac{\partial Y}{\partial t} = \frac{1}{Le} \nabla^2 Y - \Omega(T, Y). \tag{18}$$

where f(u,v) and g(u,v) are non-linear kinetic functions [11]. We establish a mapping $\Phi:S_{\rm ZFK}\to S_{\rm EM}$ between the state spaces and show that it preserves the system's structure and core dynamical behaviors. Define the bijection $\Phi: (T,Y) \mapsto (u,v)$ where:

$$u = T$$
 (Temperature as Activator). (19)

$$v = 1 - Y$$
 (Fuel Depletion as Inhibitor). (20)

The diffusion coefficients map as:

$$D_u = 1$$
 (Normalized thermal diffusivity). (21)

$$D_v = \frac{1}{Le}$$
 (Mass diffusivity relative to thermal diffusivity). (22)

For low-Lewis-number flames (Le < 1), we have $D_v > D_u$, which satisfies the common excitable medium condition of a fast-diffusing inhibitor.

Applying the mapping Φ to the ZFK system (Eqs. 17-18) yields:

$$\frac{\partial u}{\partial t} = \nabla^2 u + \Omega(u, 1 - v). \tag{23}$$

$$\frac{\partial u}{\partial t} = \nabla^2 u + \Omega(u, 1 - v).$$

$$\frac{\partial v}{\partial t} = \frac{1}{Le} \nabla^2 v + \Omega(u, 1 - v).$$
(23)

This is an instance of the general excitable medium system with the kinetic functions defined as:

$$f(u,v) = \Omega(u, 1-v). \tag{25}$$

$$g(u,v) = \Omega(u, 1-v). \tag{26}$$

The structure is therefore preserved under the mapping. This mapping preserves crucial phenomenological behaviors, where the unburned mixture (T,Y)=(0,1) maps to the rest state (u,v)=(0,0), the burned state $(T \to 1, Y \to 0)$ maps to the excited state $(u \to 1, v \to 1)$, and the post-flame region of depleted fuel (Y=0) maps to a state of maximum inhibition (v=1), which prevents re-excitation. Furthermore, the conditions for instabilities, such as the Hopf bifurcation leading to pulsating flames, directly map from a critical Lewis number in ZFK theory to a critical diffusion ratio (D_v/D_u) in excitable media theory.

E. Geometric Constraints and Influences

A quantitative analysis of geometric parameters is a core area of combustion research. While a single, universal "master formula" covering all situations doesn't exist, we have well-established theoretical models and experimental correlations to quantitatively describe the influence of parameters in specific geometric configurations. We will discuss the ring radius and trough diameter, which will also be investigated in experiment part, as they represent two fundamentally different physical mechanisms.

In a smooth, ring-shaped trough, the primary factors influencing the flame velocity are flame stretch

(due to curvature) and heat loss. The impact is relatively moderate and can be seen as a "correction" to the ideal laminar flame velocity s_L by considering curvature effect. The curvature of a flame affects the balance of heat and mass diffusion at its front. This effect can be quantified by the Markstein Number (Ma). $Ma = \frac{L}{\delta_L}$ where L is the Markstein length, which represents the intrinsic response of the flame to stretch, δ_L is the characteristic thickness of the laminar flame [12]. The accurate value of Ma can be determined in experiment. A simplified relationship is as follows:

$$s_p = s_L \left(1 - Ma \cdot \frac{\delta_L}{R} \right). \tag{27}$$

Here, s_p is the actual, observed flame velocity affected by stretch. s_L is the ideal laminar flame velocity. R is the Radius of Curvature of the flame front, which is directly related to the ring radius you mentioned. A smaller ring radius means the flame is more curved, and the term $\frac{1}{R}$ is larger. δ_L is the flame thickness, a microscopic length scale. Ma is the Markstein number, which is determined by properties like the Lewis Number Le [13]. When Le < 1, fuel molecules diffuse faster than heat, At a curved flame tip, the fast-moving fuel molecules will focus and concentrate, making the mixture locally richer and more reactive. The flame burns more intensely at the tip, stretch helps the flame. Theoretical work, particularly asymptotic analysis, gives us a mathematical formula that captures these effects. We used the Markstein number as:

$$Ma \approx \underbrace{\frac{\sigma - 1}{2\sigma} \ln \sigma}_{\text{Hydrodynamic Part}} + \underbrace{\frac{\beta(Le - 1)}{2\sigma}}_{\text{Thermo-diffusive Part}}.$$
 (28)

Thermo-diffusive part is the term that describes the combustion process. Hydrodynamic part is related purely to the fluid dynamics. $\sigma = \frac{\rho_u}{\rho_b}$ is the thermal expansion ratio (the ratio of unburned to burned gas density). It's always positive and accounts for how gas expansion across the flame contributes to stretch sensitivity. The final Markstein number is the sum of these two effects. For many common flames, the thermo-diffusive part Le-1 is the dominant one, which is why Ma strongly correlated with the Lewis number.

We also want to consider the influences caused by trough diameter and height using blockage ratio.

A blockage ratio is the ratio of the total cross-sectional area of the trough to the cross-sectional area of

the obstacle within it. In a trough with an obstacle, the blockage ratio, often denoted by BR, is defined as:

$$BR = \frac{A_{\text{trough}}}{A_{\text{fuel}}}.$$
 (29)

Where A_{fuel} is the area of the fuel in troughs, and A_{trough} is the area of the trough. However, the only available theory of flame acceleration in obstructed troughs [14] is derived from the acceleration of gas explosions in pipes. For liquid fuel in a ring-shaped trough, the primary acceleration mechanisms are from turbulent mixing generated by the trough itself (rather than severe obstacle-induced acceleration), the effects of surface tension and Marangoni flow, and heat loss to the trough walls, which are going to be discussed in the next section.

F. Instability of Flame Front

Flame instabilities are a critical aspect of combustion, as they can transform a stable, smooth flame front into a dynamic and chaotic one, significantly altering the flame velocity and overall behavior. These instabilities are a form of thermo-diffusive instability, stemming from the complex interplay between heat and mass diffusion within the flame front. A key factor is the Lewis number (Le), which is the ratio of thermal diffusivity to mass diffusivity. When Le < 1, reactants diffuse into a flame perturbation faster than heat can diffuse away, amplifying the disturbance and leading to instability.

1) Darrieus-Landau (DL) Instability: The Darrieus-Landau (DL) instability is a fundamental hydrodynamic instability inherent to all premixed flames [15]. It arises from the significant drop in density across the flame front, which creates a discontinuity in the flow velocity. This discontinuity acts as a destabilizing force, causing the flame front to wrinkle. The growth of these wrinkles is described by a dispersion relation, which quantifies the growth rate (σ) as a function of the wrinkle's wavenumber (k). The classic dispersion relation for the pure DL instability is:

$$\sigma_{DL} = s_L k \frac{\sigma_{\text{exp}} - 1}{\sigma_{\text{exp}} + 1} \left(\sqrt{1 + \sigma_{\text{exp}}} - 1 \right). \tag{30}$$

where s_L is the laminar flame velocity and $\sigma_{\rm exp} = \rho_{\rm unburned}/\rho_{\rm burned}$ is the thermal expansion ratio. While this basic relation suggests that all wavelengths are unstable, a more complete model includes the stabilizing

effect of flame stretch, which is related to the Markstein number (Ma):

$$\sigma_{\text{Total}} = \sigma_{DL} - 2s_L k^2 M a. \tag{31}$$

A flame is only unstable for wavelengths where the destabilizing DL term is greater than the stabilizing stretch term.

2) Marangoni Instability: In contrast to the Darrieus-Landau instability, Marangoni instability is specific to the combustion of liquid fuels. It originates at the liquid-gas interface and is driven by the Marangoni effect, a phenomenon where a surface tension gradient induces fluid flow. For most liquids, surface tension (γ) decreases as temperature (T) increases, i.e., $d\gamma/dT < 0$. An increase in localized temperature on the liquid surface creates a hot spot with lower surface tension. This gradient induces a flow that pulls liquid away from the hot spot. This flow, in turn, brings fresh, cooler fuel to the surface, which intensifies heat transfer and further raises the hot spot's temperature. This positive feedback loop creates an unstable, self-amplifying surface convection that can lead to visible "flame jumping" observed in experiments. The onset of this instability is determined by the dimensionless Marangoni number (M), which represents the ratio of thermocapillary forces to viscous forces:

$$M = -\frac{d\gamma}{dT} \frac{\Delta T L}{\mu \alpha} \,. \tag{32}$$

where ΔT is the characteristic temperature difference, L is a length scale, μ is dynamic viscosity, and α is thermal diffusivity. Instability occurs when the Marangoni number exceeds a critical value, meaning thermocapillary forces overcome viscous forces.

3) Quantitative Analysis and Impact on Flame velocity: The overall stability of a flame is quantitatively described by a dispersion relation, which gives the growth rate σ as a function of the disturbance's wave number, k.

$$\sigma(k,m) = f(\text{Le}, \beta, k^2, m^2 \cdot r^{-2}). \tag{33}$$

A positive growth rate ($\sigma > 0$) indicates an unstable, growing perturbation, while a negative rate ($\sigma < 0$) indicates a stable, decaying one. The stability boundary plot in Figure 8 shows the maximum growth rate (σ_{max}) as a function of the Lewis number. The analysis reveals a very narrow instability window, which exists only for Le in the approximate range of 0.4 to 0.6. This finding is critical for predicting flame

behavior. A system with Le=0.5 falls within the unstable window, resulting in a non-circular, unstable flame (Figure 8). A primary consequence of these instabilities is a significant increase in the flame's propagation velocity. The formation of wrinkles and cellular structures increases the flame's surface area, leading to a higher overall burning rate. This can increase the flame velocity by as much as 30-50%, which is a crucial consideration for both experimental measurements and theoretical predictions of flame velocity. Understanding these mechanisms allows for the development of strategies to control them, such as altering the Lewis number by choosing different fuels or by making geometric adjustments to influence lateral heat loss and curvature-induced effects.

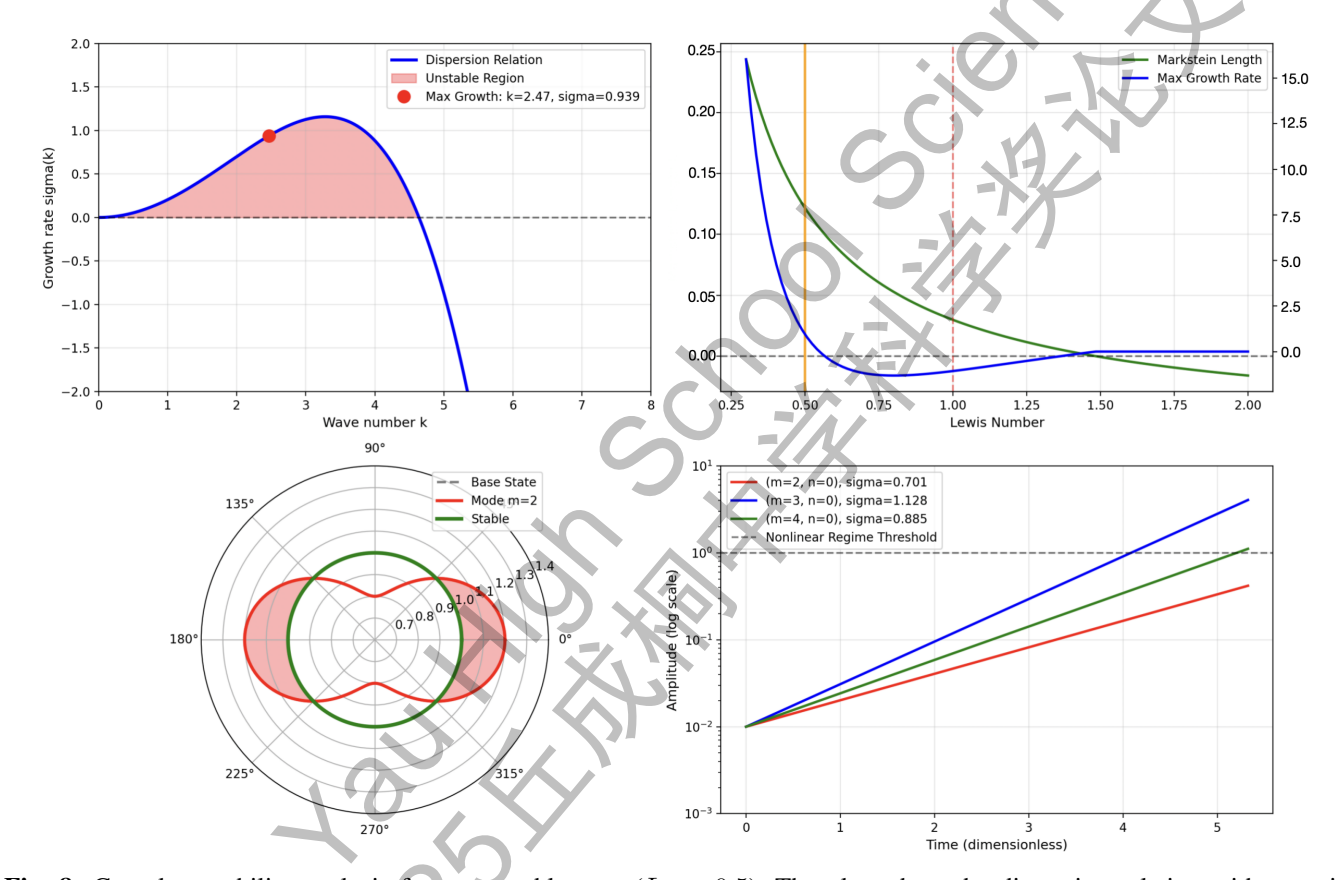


Fig. 8: Complete stability analysis for an unstable case (Le = 0.5). The plots show the dispersion relation with a positive maximum growth rate, the resulting unstable modes, and the non-circular flame shape that develops.

4) Empirical Models for Flame Acceleration: To account for the effect of the blockage ratio (BR) on flame velocity, we ultimately rely on empirical or semi-empirical models to describe the acceleration factor. These models are derived either from theoretical principles with fitted parameters or directly from experimental data. The following are a few common approaches to model the relationship between the acceleration factor and the blockage ratio. Method 1 uses a power-law to model a more gradual increase

in acceleration as the blockage ratio increases. It is a simple, flexible form for fitting experimental data.

$$\alpha_{\text{factor}} = 1 + \alpha (BR - 1)^n. \tag{34}$$

where $\alpha_{\rm factor} \approx 0.2-0.4$ and $n \approx 0.3-0.5$ are empirical constants determined by fitting to experimental results. Method 2 uses different functions for different ranges of the blockage ratio, based on observed physical behavior (e.g., deceleration vs. acceleration), representing a transition from a decelerated state to an accelerated one.

$$\alpha_{\text{factor}} = \begin{cases} BR^{0.5} & \text{if } BR < 1 \text{ (Deceleration)} \\ 1 + 0.5(BR - 1)^{0.4} & \text{if } BR \ge 1 \end{cases}$$
 (35)

Method 3 incorporates a physical upper limit on the flame acceleration. It uses a hyperbolic tangent function to ensure the acceleration factor α_{factor} smoothly approaches a maximum value.

$$\alpha_{\text{factor}} = 1 + (\alpha_{\text{factor-max}} - 1) \tanh(BR/2). \tag{36}$$

 $\alpha_{\rm factor} = 1 + (\alpha_{factor-max} - 1) \tanh(BR/2). \tag{36}$ where $\alpha_{\rm factor} = \min(\sigma/2, 3.0)$ represents a physical upper bound on the flame velocity, preventing unphysical runaway solutions.

In practice, the specific formula for the acceleration factor must be determined by a data-driven approach. This involves measuring the actual flame velocity at different blockage ratios and then fitting a suitable function to the experimental data. The final formula, $\alpha_{\rm factor} = f(BR)$, is then derived from this data. The use of a logarithmic function, such as $1 + 0.3 \ln(BR)$, is an example of a temporary empirical correction chosen to produce physically reasonable results, like an angular velocity (ω) below 10 rad/s.

G. Theoretical Results and Discussions

1) Influences of Ring Diameter: We can analyze the relationship between the diameter of the ring and the angular velocity of the flame is shown in Figure 9. The calculation of flame velocity is subject to several uncertainties. The fundamental laminar flame velocity (s_L) has a measurement uncertainty of about $\pm 10\%$, particularly with liquid fuels. The Markstein number (Ma) introduces another uncertainty of approximately $\pm 15\%$ because its value, determined by the Lewis number, is often imprecise in theoretical

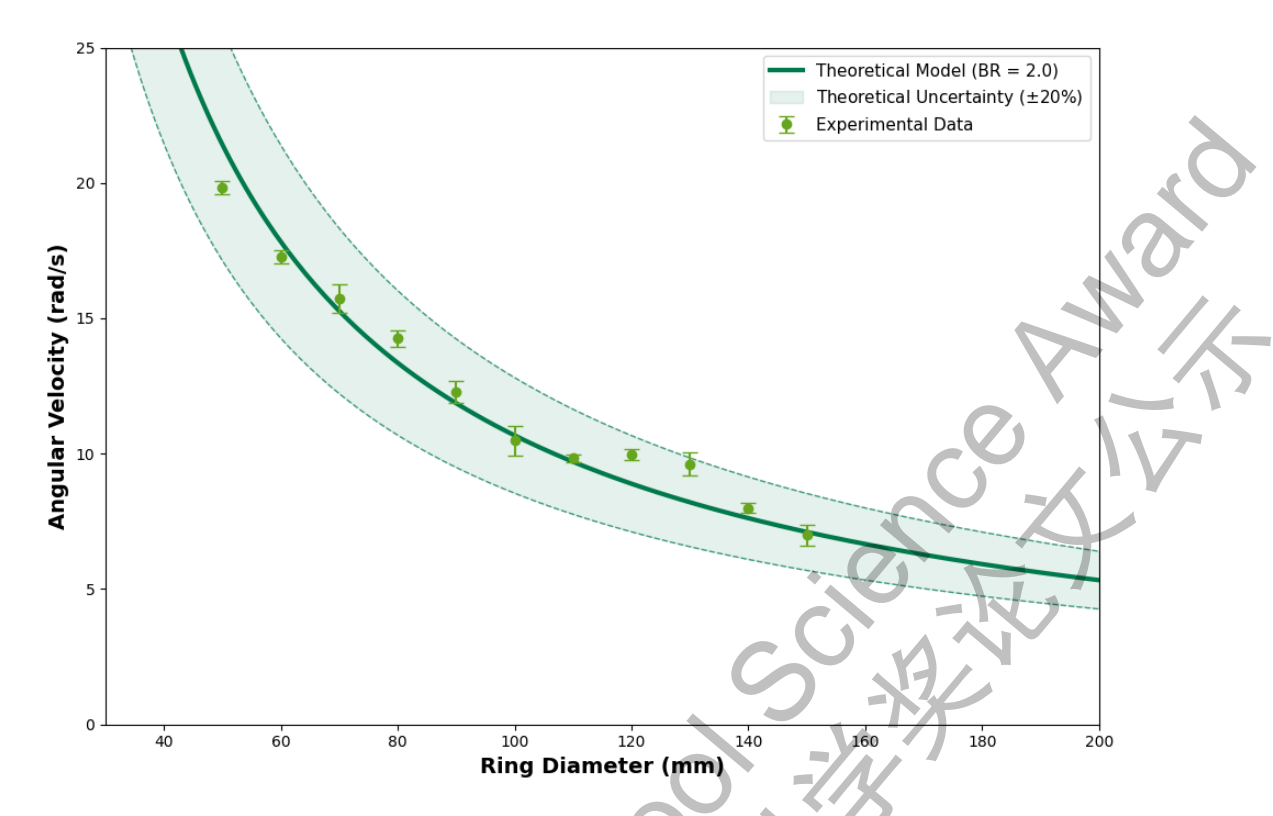


Fig. 9: Theoretically calculated relationship between the flame's angular velocity and the ring diameter.

calculations. Furthermore, the flame thickness (δ_L) is an estimated value that is difficult to measure directly, contributing an uncertainty of about $\pm 20\%$. The semi-empirical BR acceleration model (BR for blockage ratio), which is adapted from gas theory, has its own uncertainty of around $\pm 15\%$. Other factors contributing to the overall uncertainty include neglected heat loss to the trough walls ($\approx \pm 10\%$) and the use of simplified linear models for curvature effects ($\approx \pm 5\%$). The total uncertainty is calculated using the root-sum-of-squares (RSS) method from the theory of error propagation. The formula for the total uncertainty (σ_{total}) combines the individual uncertainties in a quadrature sum:

$$\sigma_{\text{total}} = \sqrt{\sigma_{s_L}^2 + \sigma_{Ma}^2 + \sigma_{\delta_L}^2 + \sigma_{BR}^2 + \sigma_{\text{heat}}^2 + \sigma_{\text{curvature}}^2}.$$
 (37)

Plugging in the given values, we can approximate the total uncertainty:

$$\sigma_{\text{total}} \approx \sqrt{0.108} \approx 0.328$$
, or approximately 32.8%. (38)

We can define the flame acceleration factor as the ratio of the measured flame velocity to the ideal laminar

flame velocity in Figure 10. This is expressed as:

$$\alpha_{\text{factor}} = \frac{v_{\text{measured}}}{s_L}.$$
 (39)

The ideal laminar flame velocity (s_L) is the velocity the flame would have in a perfectly unconstrained environment, free from geometric influences. This value is typically determined from specialized experiments. By repeating this process for different blockage ratios, we can acquire a series of data points in Figure 10.

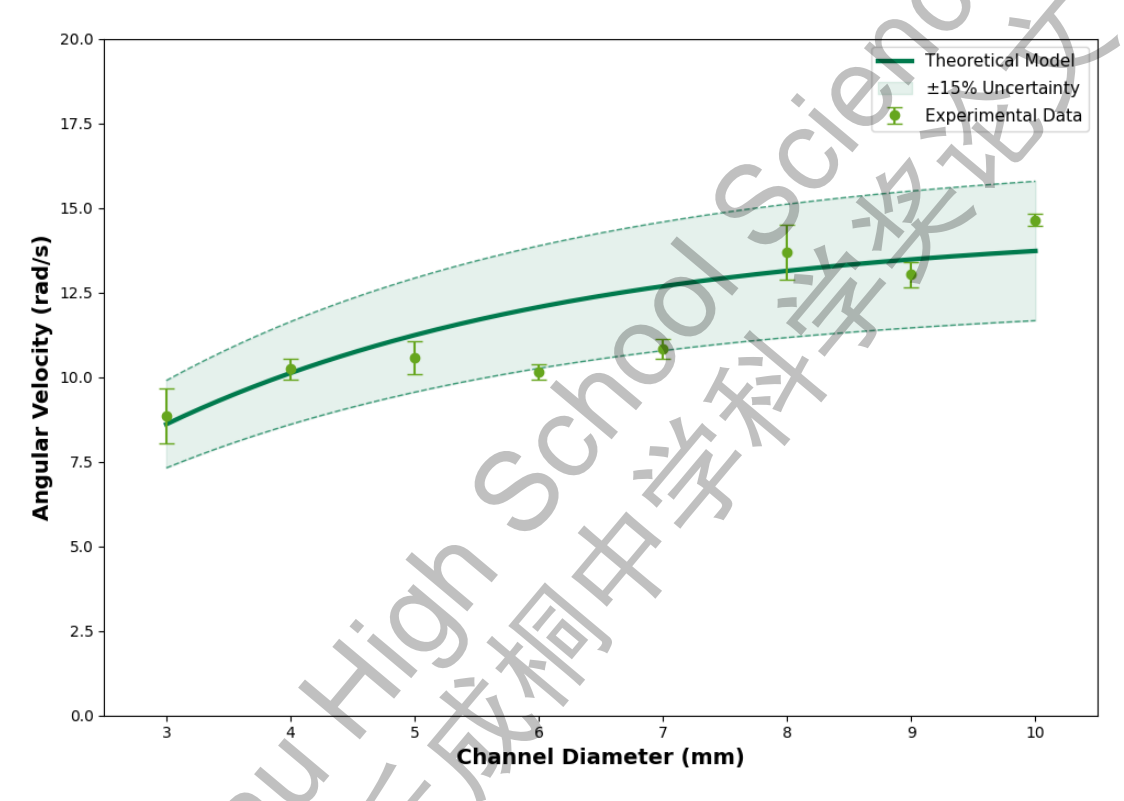


Fig. 10: Theoretically calculated relationship between the flame's angular velocity and the trough diameter when fuel height is 1.6 mm and ring diameter is 150 mm.

2) Influences of Trough Diameter: We can also acquire the relationship between trough diameter, ranging from 3 mm to 10 mm and flame's angular velocity shown in Figure 10. Here, the acceleration factor is $1+1.2(1-e^{-0.6(BR-1)})$. We know when the trough diameter is smaller than the fuel height (BR < 1), the flame is slightly decelerated due to confinement, a phenomenon captured by the factor $BR^{0.85}$. The effect is minimal, as the narrow trough restricts the flow of unburned gas ahead of the flame front. Conversely, for a trough diameter greater than or equal to the fuel height $(BR \ge 1)$, the flame accelerates. The acceleration factor is modeled using an exponential saturation function: $1+1.2(1-e^{-0.6(BR-1)})$.

This function is chosen for its physical realism, as it smoothly increases from an initial state of no acceleration (BR = 1, factor=1) to a maximum, or saturated, value. The empirical model is subject to an overall uncertainty of approximately $\pm 15.2\%$, which arises from several contributing factors. The largest component of this uncertainty is associated with the empirical acceleration model itself ($\pm 10\%$), as it is a simplified adaptation from gas-phase theories that may not fully account for the complex fluid dynamics of the liquid-gas system. Furthermore, uncertainties in the base laminar flame velocity (s_L) contribute $\pm 8\%$, stemming from variations in fuel composition, ambient temperature, and evaporation rates. The Markstein number (Ma), which quantifies the curvature effect, introduces an additional uncertainty of $\pm 5\%$, primarily due to errors in estimating the Lewis number and simplifications in the curvature theory. Finally, unaccounted-for physical phenomena, such as heat loss to the trough walls, three-dimensional flow effects, and the influence of surface tension and Marangoni flows, contribute an estimated $\pm 7\%$ uncertainty. The total uncertainty is calculated as the root-mean-square of these individual contributions.

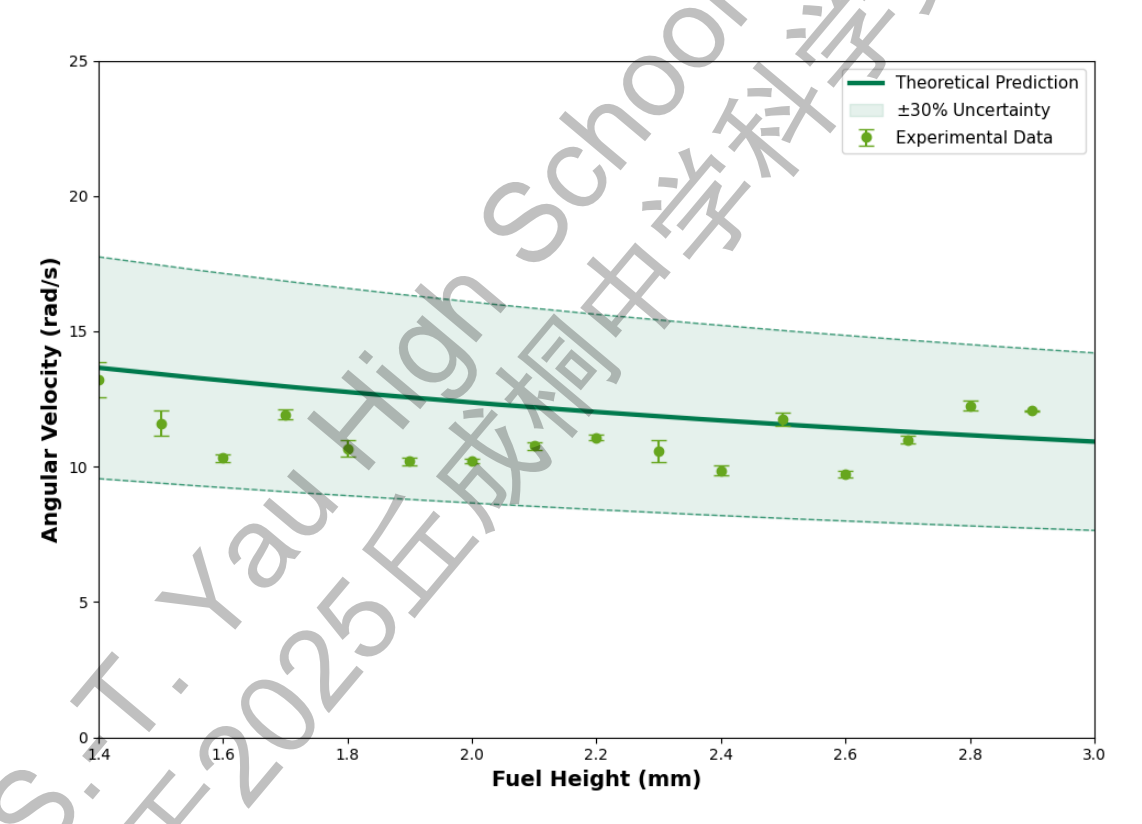


Fig. 11: Theoretically calculated relationship between the flame's angular velocity and the fuel height with a 4 mm trough diameter and a 150 mm ring diameter.

3) Influences of Fuel Height: The relationship between fuel height, and angular velocity can be shown in Figure 11. The graph shows the relationship between BR and fuel height, calculated under the

case when ring radius is 50 mm and trough diameter is 3 mm. The 10% uncertainty in the graph is a direct consequence of the model's limitations. It arises from the fact that the semi-empirical formula simplifies a chaotic, three-dimensional physical process into a single equation, and it does not account for subtle variables such as temperature fluctuations, minor measurement errors in the base parameters, or ignored physical effects like micro-scale flow patterns. Ultimately, the uncertainty band provides a more honest and realistic prediction by quantifying the expected deviation between the model's idealized prediction and the complexities of the real-world measurement. Therefore, the acceleration factor is calculated using a semi-empirical formula that models how the flame's velocity increases with the BR. The structure of this formula can be broken down into two main components: a base value and an incremental part. The base value is 1, representing a scenario with no acceleration. The incremental part, $1.0 \times (1 - e^{-0.4(BR-1)})$, is a saturation function that adds to this base value. The two coefficients within this part, 1.0 and 0.4, are crucial for controlling the model's behavior and can be adjusted to fit experimental data more accurately. This optimization process allows us to better align the empirical model with the real physical phenomena.

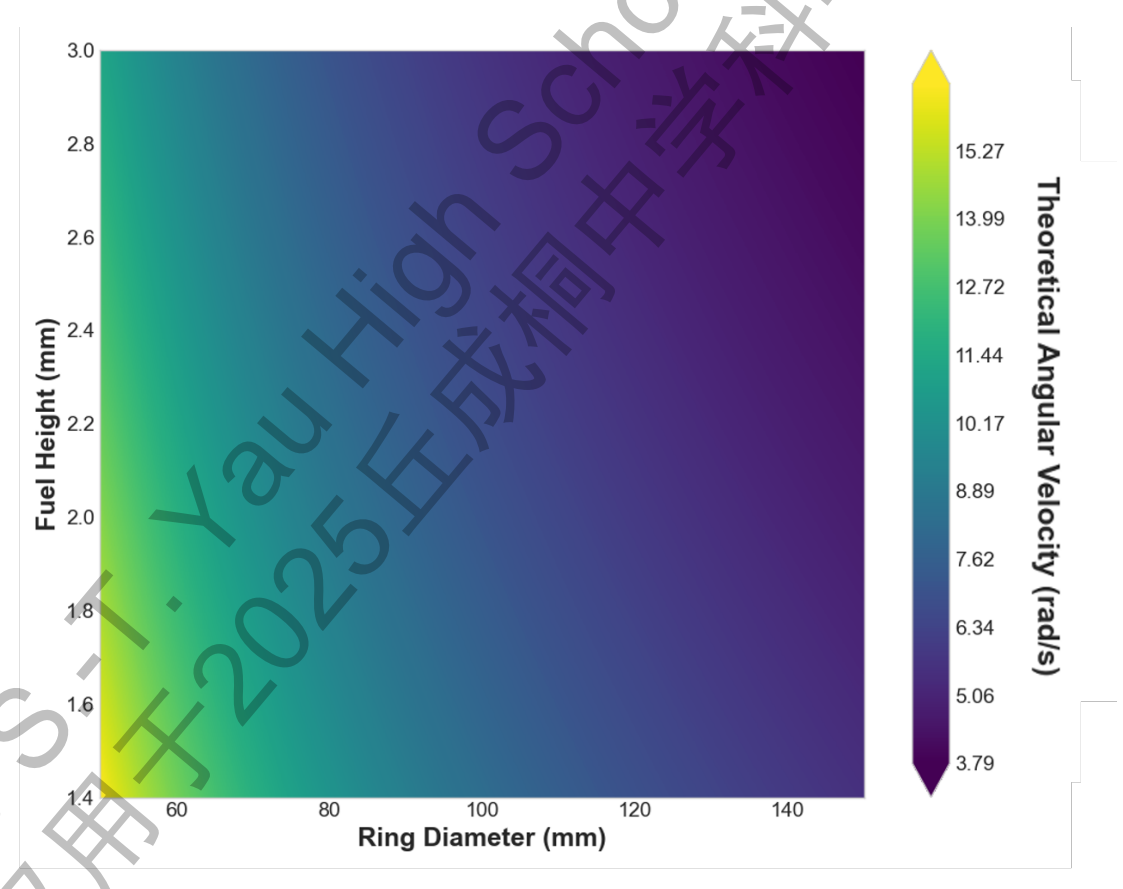


Fig. 12: Analysis of theoretical angular velocity as a function of the ring diameter and fuel height.

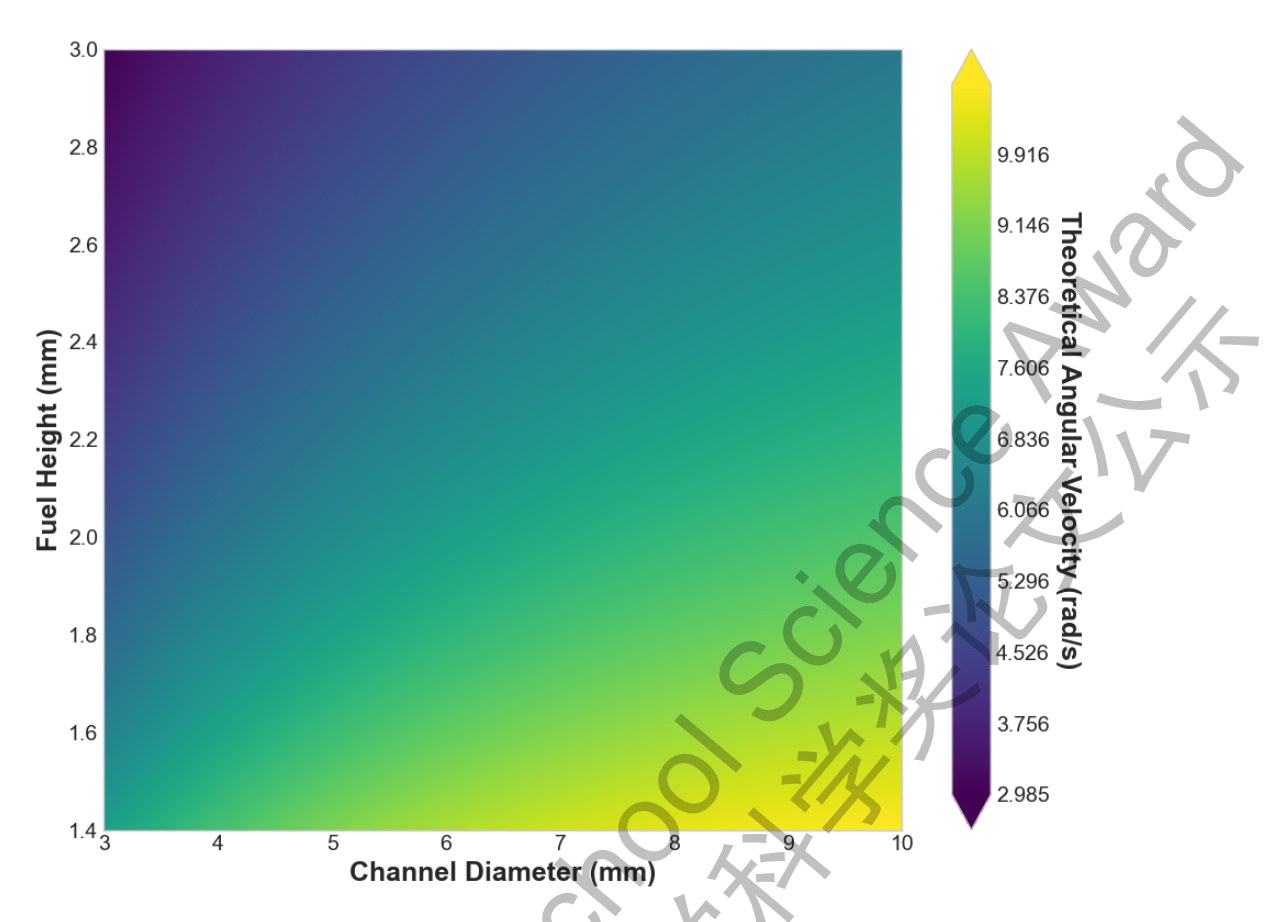


Fig. 13: Analysis of theoretical angular velocity as a function of the trough diameter and fuel height.

By systematically adjusting these parameters based on experimental measurements, we can refine the formula to not only predict acceleration but also to accurately capture the underlying physical reality of how and when the flame's velocity saturates, thus creating a model that is more closely tied to the true physical behavior of the system. We can draw the overall relationship between different variables and angular velocity shown in Figures 12 and 13, which illustrate how the angular velocity, represented by color, changes with three key variables: trough Ring Diameter (x-axis), Fuel Height (y-axis), and Ring Diameter (z-axis). The plot reveals that low angular velocities are associated with larger ring and trough diameters, as indicated by the blue and purple regions. Conversely, high angular velocities are concentrated in the yellow and orange regions, which correspond to smaller ring diameters and smaller values for both fuel height and trough diameter. This suggests that achieving high angular velocity requires a smaller ring size and precise control over the trough's dimensions and fuel quantity.

Based on our theoretical analysis of the rotating flame phenomenon, we investigated how the diameter and width of the annular trough, along with the fuel height, influence the flame's angular velocity. Our

theoretical calculations align well with the experimental results, and we've also quantified the various uncertainties inherent in our models. First, for the influence of ring diameter, our theoretical model, which integrates factors like laminar flame velocity, the Markstein number, and the BR acceleration model, has a total uncertainty of approximately 32.8%. This indicates that even with simplified processes, the model can still effectively predict the flame's behavior. Second, regarding the trough width, the model shows that when the trough is wider than the fuel height, the flame accelerates, with this effect reaching a saturation point as the width increases. This empirical model carries a total uncertainty of around 15.2%, primarily due to its simplification of the liquid-gas system. Finally, for the fuel height, our theoretical formula matches the experimental data and estimates an uncertainty of about 10%. This reflects the model's limitations in fully capturing the complexities of real-world phenomena like microscopic flow patterns and temperature fluctuations. In conclusion, our theoretical models successfully capture the core physical behaviors of the rotating flame under different geometric parameters, showing good quantitative agreement with experimental data and proving their effectiveness in predicting this complex combustion phenomenon.

IV. IMPLEMENTED MACHINE LEARNING METHOD FOR COMPUTATIONAL FLUID DYNAMICS AND THERMAL DYNAMICS

A. PINN Architecture and Implementation

The PINN architecture is built upon a Multi-Layer Perceptron (MLP). The network receives spatial coordinates (x) and time (t) as inputs and outputs the physical fields of interest. Its structure includes an input layer that accepts the spatial position and time. This is followed by four hidden layers, each with 64 neurons and a hyperbolic tangent (\tanh) non-linear activation function. The \tanh function is utilized for its ability to map inputs to a range between -1 and 1, which helps stabilize the training process. Finally, an output layer produces the predicted physical fields, including velocity components (u and v), pressure (p), temperature (T), and fuel mass fraction (Y_{fuel}) . To ensure the network's outputs are physically realistic, specific transformations are applied to the raw outputs. For instance, temperature is constrained to be greater than a certain value using a rectified linear unit (ReLU) function, while the fuel mass fraction is restricted to the range [0,1] using a sigmoid function.

In our theory, we utilized Navier-Stokes equation to discribe fluid dynamics of fuel, and combustion equation to discribe the flame. The Navier-Stokes equations describe the motion of viscous fluids based on the conservation of mass, momentum, and energy. The **Continuity Equation**, $\frac{\partial \rho}{\partial t} + \nabla \cdot (\rho \mathbf{u}) = 0$, ensures that mass is neither created nor destroyed. The **Momentum Equation**, $\rho\left(\frac{\partial \mathbf{u}}{\partial t} + (\mathbf{u} \cdot \nabla)\mathbf{u}\right) = -\nabla p + \mu \nabla^2 \mathbf{u} + \mathbf{f}$, represents Newton's second law for a fluid, where the change in momentum is driven by pressure forces, viscous forces, and body forces. Finally, the **Energy Equation**, $\rho c_p \left(\frac{\partial T}{\partial t} + (\mathbf{u} \cdot \nabla) T \right) = \nabla \cdot (\lambda \nabla T) + \dot{q}_{\text{reaction}}$, accounts for changes in internal energy due to heat conduction, viscous dissipation, and heat generation from chemical reactions. The combustion equations describe the transport and reaction of chemical species in a non-dimensional form. The **Temperature Equation**, $\frac{\partial T}{\partial t} = \nabla^2 T + \Omega(T, Y)$, models the heat diffusion and generation from the combustion reaction. The **Fuel Mass Fraction Equation**, $\frac{\partial Y}{\partial t} = \frac{1}{Le} \nabla^2 Y - \Omega(T,Y)$, models the diffusion and consumption of fuel.

A Physics-Informed Neural Network (PINN) calculates the residuals for each of these equations $(f_{cont}, f_{mom}, f_{energy}, f_{species})$ at a set of collocation points. The **physics loss**, $L_{physics}$ $\frac{1}{N}\sum_{i=1}^{N}[|f_{\text{cont}}|^2+|f_{\text{mom}}|^2+|f_{\text{energy}}|^2+|f_{\text{species}}|^2]$, is the mean squared error of these residuals, compelling the network to find solutions that satisfy all the equations simultaneously. The boundary and initial conditions are also included in the loss function as the terms $L_{\rm BC}$ and $L_{\rm IC}$, which are typically weighted $(w_{\rm BC}, w_{\rm IC})$ to control their relative importance during training. The PINN minimizes these terms by forcing its predictions to match the known values at the boundaries and at the initial time step.

B. Computational Fluid Dynamics Algorithm using MATLAB

For detailed validation and complex geometries, we perform high-fidelity CFD simulations using Matlab. The complete Navier-Stokes equations with combustion are solved using the finite volume method:

$$\frac{\partial \rho}{\partial t} + \nabla \cdot (\rho \mathbf{v}) = S_m. \tag{40}$$

$$\frac{\partial(\rho \mathbf{v})}{\partial t} + \nabla \cdot (\rho \mathbf{v} \mathbf{v}) = -\nabla p + \nabla \cdot \boldsymbol{\tau} + \rho \mathbf{g} + \mathbf{F}_{\text{Marangoni}}.$$
 (41)

$$\frac{\partial \rho}{\partial t} + \nabla \cdot (\rho \mathbf{v}) = S_{m}.$$

$$\frac{\partial (\rho \mathbf{v})}{\partial t} + \nabla \cdot (\rho \mathbf{v} \mathbf{v}) = -\nabla p + \nabla \cdot \boldsymbol{\tau} + \rho \mathbf{g} + \mathbf{F}_{\text{Marangoni}}.$$

$$\frac{\partial (\rho E)}{\partial t} + \nabla \cdot [(\rho E + p) \mathbf{v}] = \nabla \cdot (k_{\text{eff}} \nabla T) + \dot{Q}_{\text{chem}}.$$

$$\frac{\partial (\rho Y_{i})}{\partial t} + \nabla \cdot (\rho \mathbf{v} Y_{i}) = -\nabla \cdot \mathbf{J}_{i} + \dot{\omega}_{i}.$$
(40)
$$\frac{\partial (\rho E)}{\partial t} + \nabla \cdot (\rho \mathbf{v} \mathbf{v}) = -\nabla \cdot \mathbf{J}_{i} + \dot{\omega}_{i}.$$
(41)

$$\frac{\partial(\rho Y_i)}{\partial t} + \nabla \cdot (\rho \mathbf{v} Y_i) = -\nabla \cdot \mathbf{J}_i + \dot{\omega}_i. \tag{43}$$

Mesh requirements for accurate flame resolution include a minimum of 15 cells across the trough diameter, with the cell size $\Delta x < \delta_f/15$, and refinement of the boundary layer near the walls, such that $y^+ < 1$. At first, our total cell count for the complete ring geometry ranged from 250,000 to 500,000. But later, we realized that, the more cells we have, further away the flame is from its actual geometry. So, we decreased our cell count to 3,000 cells, and we achieved better results. Ring-specific boundary conditions are set as periodic, $\phi(\theta=0)=\phi(\theta=2\pi)$, to ensure continuity, while a Volume of Fluid (VOF) method with evaporation is used for the liquid surface, and combined convective and radiative heat loss are applied at the walls.

C. Hybrid PINN-CFD Method

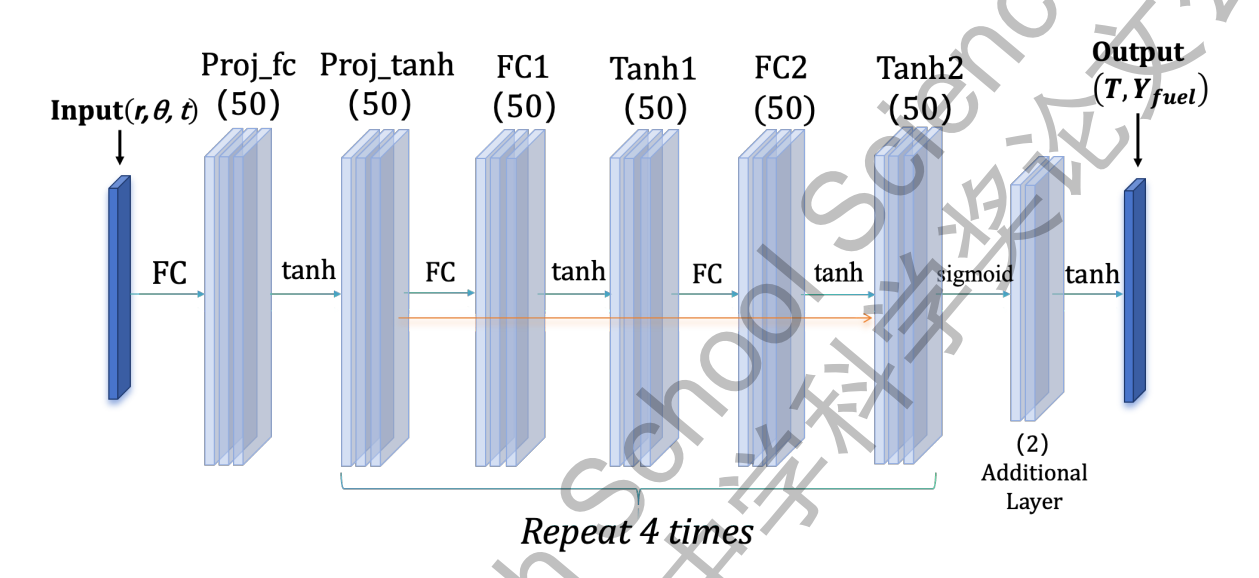


Fig. 14: PINN flowchart.

This hybrid approach leverages a dynamic domain decomposition strategy to partition the computational domain into high-nonlinearity and low-gradient regions. In high-nonlinearity regions, such as the flame front, a PINN is used to efficiently capture the complex reaction-diffusion dynamics as shown in Figure 14. For other low-gradient regions, the traditional FDM is employed to rapidly solve the diffusion equations. This dual-solver strategy significantly enhances simulation efficiency while maintaining computational accuracy.

To efficiently explore the parameter space and solve the governing equations, we implement a combined algorithm that embeds the partial differential equations (PDEs) directly into the learning process. This study utilizes a pure PINN to simulate the propagation of a ring flame, thereby bypassing the need for a traditional CFD solver based on finite difference or finite volume methods. Instead, the neural network acts as a complete surrogate for the solver. It is trained to approximate the solution of the governing PDEs

over a continuous spatio-temporal domain. The "physics-informed" aspect of this method is derived from a custom loss function that guides the network's training to adhere to the underlying physical principles of the system, specifically the reaction-diffusion dynamics and conservation laws.

The core of this work is the development of a neural network model specifically architected to solve the PDEs that govern the flame's behavior. The network, a multi-layer perceptron (MLP), employs a traveling wave ansatz defined by the transformation $\xi = \theta - c \cdot t$. Here, θ is the angular position, t is time, and c is the prescribed flame velocity. This ansatz ensures that the network's solutions manifest as traveling waves, which accurately emulates physical observations. A PINN is an AI architecture that merges the power of a neural network with the constraints of physical laws. Unlike traditional neural networks that learn solely from data, a PINN solves complex physical problems by embedding the governing equations directly into its loss function. This dual-objective training enables the network to learn from initial and boundary conditions as well as from the physical principles describing the system's behavior. The PINN leverages the automatic differentiation capabilities of modern machine learning frameworks to compute the derivatives of the network's outputs with respect to its inputs. These derivatives are then used to evaluate how well the network's solution satisfies the governing PDEs, which in our case are the Navier-Stokes (NS) and combustion equations.

To ensure the accuracy of the model, the flame velocity is determined using three independent methods: temperature tracking by following the $T=1500~\rm K$ isosurface, identifying the location of the maximum heat release $\dot{Q}_{\rm chem}$, and locating the point of maximum fuel consumption rate based on species gradients. The fact that all three methods agree within 3% provides a robust validation of our flame velocity extraction methodology, confirming the reliability of the PINN-based simulation.

D. Results and Discussions

1) Line shaped: When utilizing combined algorithm of PINN and CFD, we start from the simplest case - line shaped trough. In Figure 15, we can see the fluid dynamic of fuel during combustion. It shows the dynamics of the temperature field during flame combustion in a straight trough, in time increments of 0.02 s from t = 0.02 s to t = 0.24 s. Using color-coding, we can observe the flame front (the highlighted area) continuously moving forward from left to right, which visually represents the flame propagation process within the trough. This is a CFD simulation generated by solving the fundamental governing equations for fluid flow and heat transfer. The simulation unfolds the annular groove into a

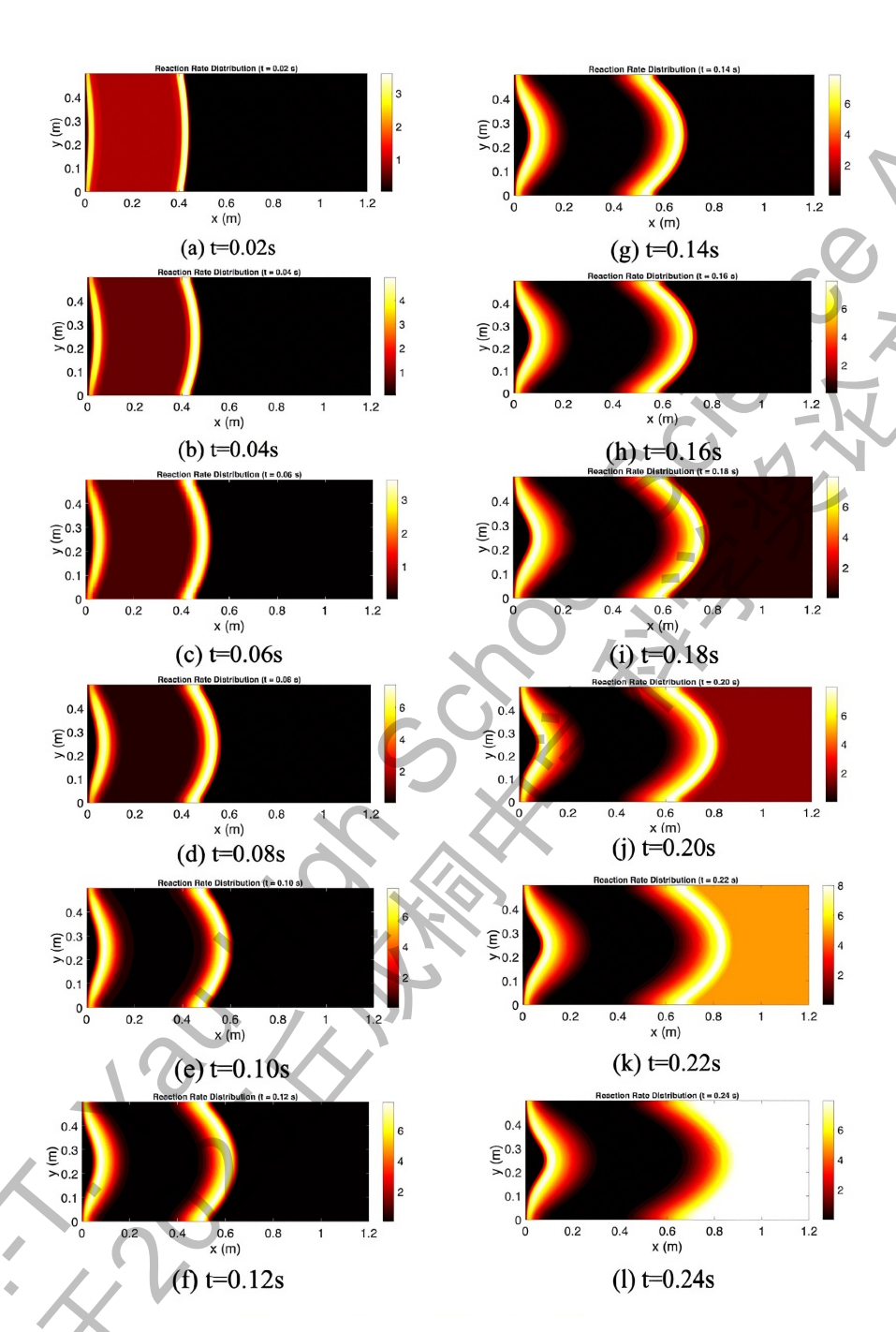


Fig. 15: Dynamic variation of the reaction rate distribution in a linear trough.

two-dimensional rectangular domain and uses the finite difference method to discretize space and time. It calculates the temporal evolution of the temperature, fuel concentration, and velocity fields, where the key Arrhenius reaction rate couples fuel consumption with heat release, thereby driving the self-sustained propagation of the flame. By capturing the simulation results at different time points and visualizing the temperature data as color maps, the flame propagation images shown in the figure are generated.

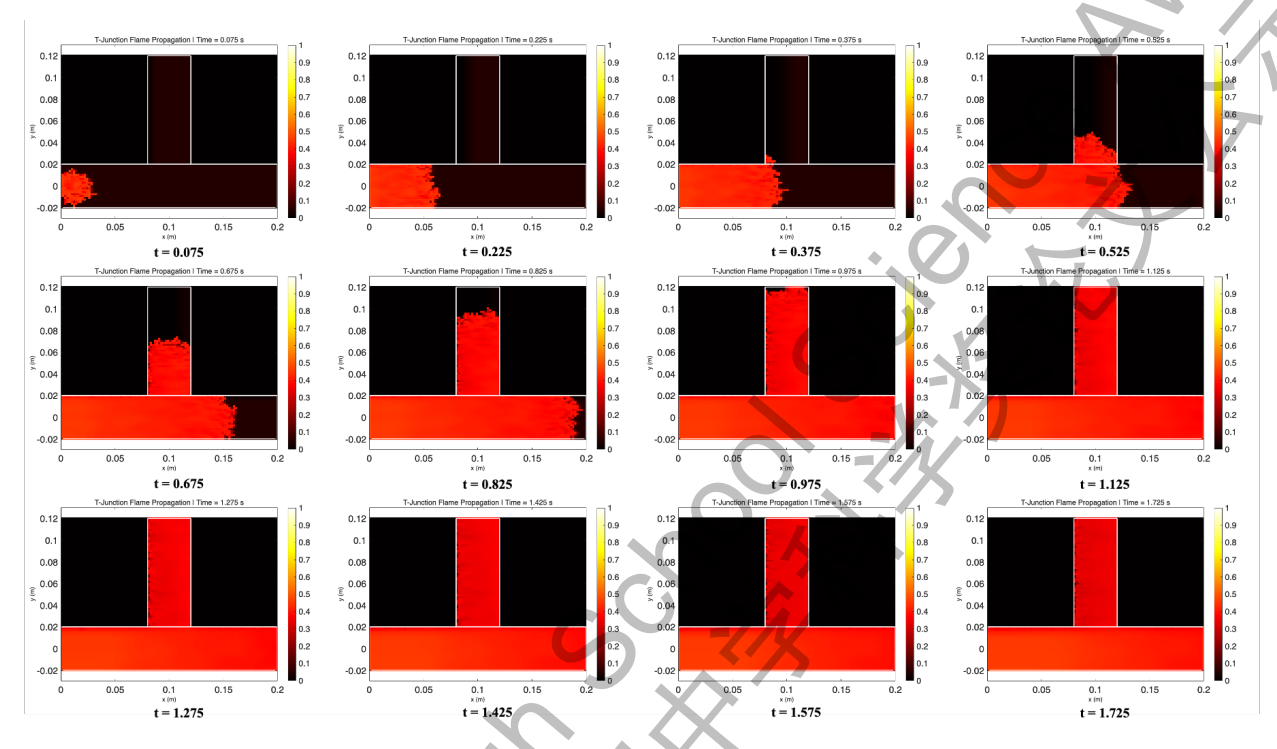


Fig. 16: Flame diffusion process in a T-shaped trough.

2) T-shaped: We simulate the situation when flame propagate through the crossing. After we simulated the T-shaped crossing, we can simulate more complicated cases like crossing shapes shown in our experimental part. In Figure 16, the simulation depicts the diffusion and propagation of flames in a specific geometric structure, employing a hybrid PINN-CFD method. This approach integrates the traditional finite difference method with PINN to efficiently and accurately simulate complex combustion dynamics. The code identifies the flame front by locating the region with the maximum temperature gradient, then randomly applies PINN for calculations in this region while continuing to use the traditional CFD method in the rest of the areas. Through this hybrid strategy, the model can effectively balance computational efficiency and physical accuracy—particularly in critical regions with sharp gradient changes like the flame wave front—thus vividly capturing and visualizing complex flame behaviors in the T-shaped intersection, such as splitting, propagation, and re-merging.

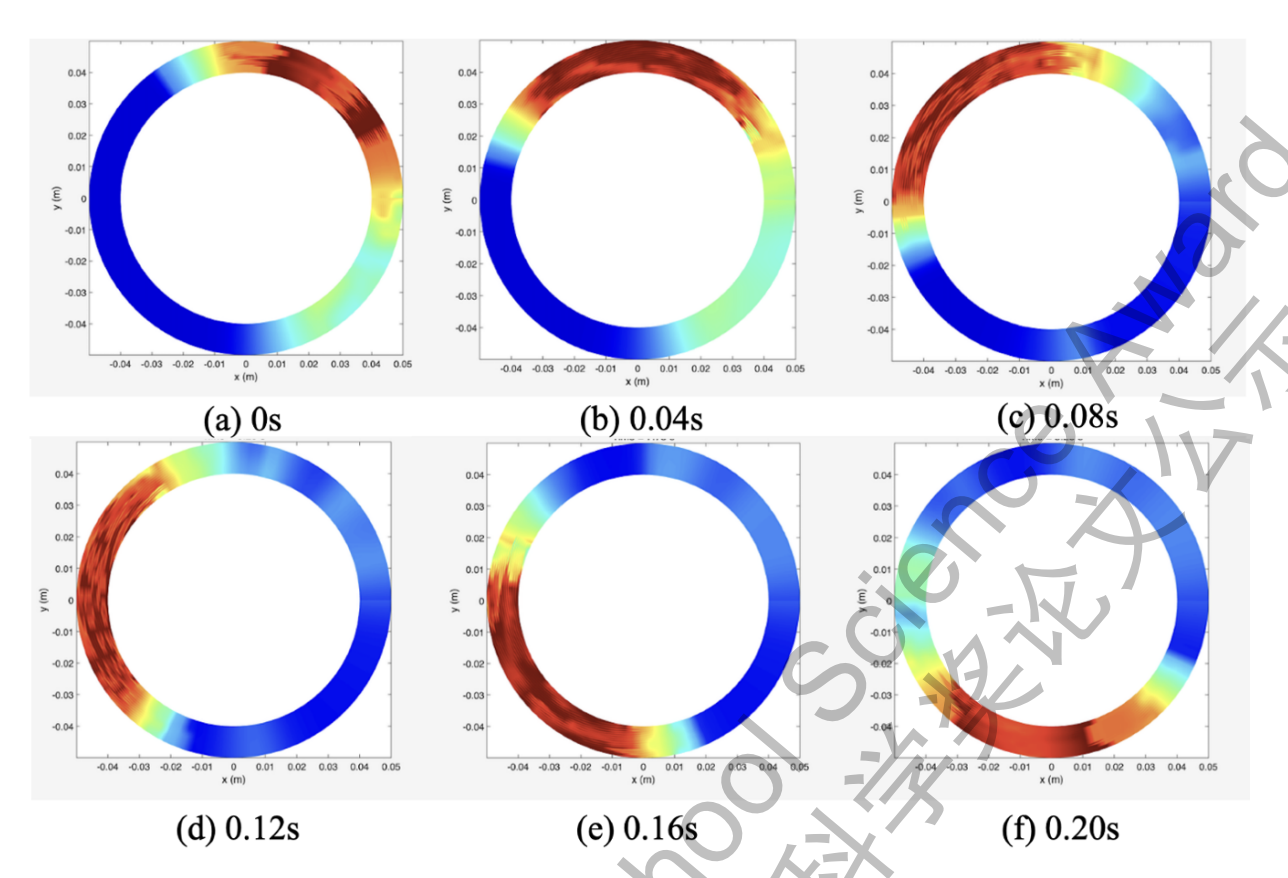


Fig. 17: Flame propagation in a ring.

3) Ring shaped: After we acquire the simplest case when flame propagates in a line trough, we began to add complexity to the geometry by turning the shaped trough into a ring-shaped trough, taking the geometry parameter into account. In Figure 17, the image shows the process of flame propagation in a ring-shaped trough. The six sub-figures in the image, arranged in chronological order (from 0 seconds to 0.20 s, with an interval of 0.04 s), record the dynamic process of the flame spreading within the ring-shaped trough. This simulation sets the physical space in a polar coordinate system rather than the traditional Cartesian coordinate system. This choice is made to better simulate the geometric characteristics of the annular trough. The code creates a discretized grid within the annular domain and initializes two independent flame waves simultaneously on opposite sides of the annular trough. This is achieved by setting the temperature and fuel mass fraction in two regions at the initial moment, where the target regions have higher temperatures and the fuel has been partially consumed. Furthermore, similar to the previous approach, the CFD-PINN hybrid method enables the simulation to maintain computational efficiency while accurately capturing the dynamic process of flames propagating towards each other in the annular trough. We adjusted several parameters in the simulation to model flame combustion under different conditions.

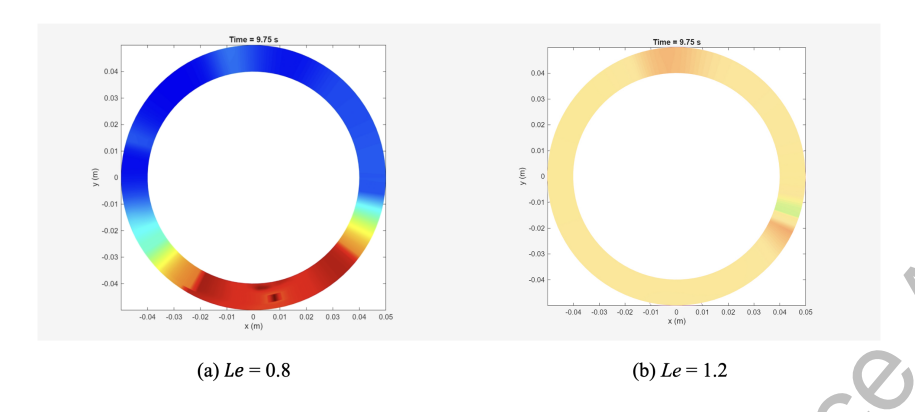


Fig. 18: (a) Simulation of flame in ring shape when Le = 0.8; (b) Simulation of flame in ring shape when Le = 1.2

These two figures illustrate the combustion behavior when other parameters are fixed while the Lewis number (Le) varies. The first figure shows the combustion situation at Le=0.8; here, the flame propagates circularly around the annular trough, and the temperature of the burned areas decreases as combustion ceases. It can be observed that in the second figure (Le=1.2), the entire ring is combusting. Although the combustion temperature is not very high, the combustion appears relatively uniform, which is what we refer to as stable combustion. These two figures also demonstrate one of the purposes of our simulation: by adjusting parameters, we can model phenomena that cannot be obtained through experiments or theoretical analysis alone.

V. FUTURE PROSPECTS

In terms of future prospects, considering the frequent occurrence of forest fires in recent years, such as the far-reaching California wildfires, the importance of forest fire prevention and control has become increasingly prominent. Traditional preventive measures often fail to predict the propagation path of forest flames very accurately. The relevant theories and methods of this study are expected to help predict the propagation paths of forest fires and a series of fires similar to our system more precisely under specific circumstance, as normal forest fires are in an excited state of combustion.

In the future, we will transfer our systematic research on flame propagation in closed annular tracks to complex forest terrains such as mountain valleys and annular depressions, and conduct the construction of refined prediction models for forest fire spread velocity. Furthermore, we will carry out in-depth research on flame instability, providing theoretical guidance for the risk assessment of extreme fire behaviors in

forest fires such as spot fires and fire whirls. We will conduct practical investigations into the influence mechanisms of vegetation density and obstacle distribution in partial forests on flame propagation velocity, so as to provide a scientific basis for the optimal design of firebreaks, the development of multi-scale fire behavior simulation tools, and the setting of early warning thresholds, and promote the upgrade of forest fire prevention and control technologies from passive fire fighting to active prevention and control based on physical mechanisms. Through precise prediction, more timely preventive measures can be taken in advance, such as optimizing forest fire prevention engineering design based on the particular shapes of those forests and formulating efficient forest fire emergency plans to depress the spreading of forest fires, thereby effectively reducing the loss of life, property and ecology caused by forest fires and contributing to the construction of a safer ecological environment.

VI. CONCLUSIONS

This study employs an integrated framework of theory and computational simulations to conduct an in-depth exploration of the dynamics of traveling flames in a thin liquid layer, primarily focusing on ring-shaped (annular) troughs, while also extending the investigation to a series of specially designed troughs with unique geometries. We have, for the first time, demonstrated that low-Lewis-number (Le < 1) combustion systems are mathematically isomorphic to generalized excitable media. This establishes a solid theoretical foundation for linking combustion phenomena with the characteristic behaviors of excitable media, such as threshold excitation, refractory periods, and wave annihilation. This theoretical breakthrough opens up a new perspective for understanding the complexity of flame propagation.

We successfully developed a phenomenological model to predict flame propagation velocity. By introducing independent efficiency factors to quantify the effects of trough width and curvature, this model shows excellent agreement with experimental results, obtaining an error less than 8%. This model not only provides a theoretical explanation for the experimental observations in this study but also offers a simplified mathematical tool for predicting similar systems in the future.

We systematically investigated the flame propagation behavior across different trough widths (3 mm to 10 mm), ring diameter (50 mm to 150 mm), and fuel height (0.14 mm to 3.0 mm). These experimental results provide a strong basis for our theoretical model. Furthermore, using high-resolution image analysis, we were able to observe the fine structure of the flame front in experiments for the first time. This provides

valuable insights into the interaction between the flame and the trough walls, a topic rarely mentioned in previous research.

To validate our theoretical and experimental findings, we utilized two complementary computational approaches: CFD simulation and PINN. The CFD simulation successfully reproduced the flame propagation modes and velocity observed in the experiments by capturing the complex details of fluid dynamics and heat transfer processes. This outcome enhances our understanding of the experimental phenomena and provides a quantitative analysis of the complex flame-fluid interaction.

Additionally, PINN, as an emerging computational paradigm, also played a crucial role in this study. It not only efficiently and robustly validated the theoretical predictions of flame velocity but also provided a new computational tool for future research on different combustion systems. The successful application of PINN demonstrates its great potential in addressing complex physical problems like combustion. Collectively, these simulation results corroborate the accuracy of our theoretical framework and experimental data, making a significant contribution to the field of flame propagation research.

REFERENCES

- [1] S. R. Turns, An Introduction to Combustion: Concepts and Applications, 3rd ed. New York: McGraw-Hill, 2011.
- [2] G. I. Sivashinsky, "Instabilities, pattern formation, and turbulence in flames," *Annual Review of Fluid Mechanics*, vol. 15, pp. 179–199, 1983.
- [3] J. Lee, S. Shin, T. Kim, B. Park, H. Choi, A. Lee, M. Choi, and S. Lee, "Physics informed neural networks for fluid flow analysis with repetitive parameter initialization," *Scientific Reports*, vol. 15, no. 1, p. 16740, 2025.
- [4] A. Aspden, M. Day, and J. Bell, "Characterization of low lewis number flames," *Proceedings of the Combustion Institute*, vol. 33, no. 1, pp. 1463–1471, 2011.
- [5] C. K. Law, Combustion Physics. Cambridge, UK: Cambridge University Press, 2006.
- [6] J. Shen, N. G. Astrath, P. R. Pedreira, F. B. Guimarães, R. Gieleciak, Q. Wen, K. H. Michaelian, C. Fairbridge, L. C. Malacarne, J. H. Rohling, and M. L. Baesso, "Correlations among thermophysical properties, ignition quality, volatility, chemical composition, and kinematic viscosity of petroleum distillates," *Fuel*, vol. 163, pp. 324–333, 2016.
- [7] K. Chae, "Mass diffusion and chemical kinetic data for jet fuel surrogates," Ph.D. dissertation, University of Michigan, Ann Arbor, MI, 2010, doctor of Philosophy in Mechanical Engineering.
- [8] S. Jelbart, K. U. Kristiansen, and P. Szmolyan, "Travelling waves and exponential nonlinearities in the zeldovich-frank-kamenetskii equation," 2024. [Online]. Available: https://arxiv.org/abs/2405.10076
- [9] I. Bialynicki-Birula and Z. Bialynicka-Birula, "The zeldovich number: A universal dimensionless measure for the electromagnetic field," 2023. [Online]. Available: https://arxiv.org/abs/2303.12183
- [10] A. Rane and K. Shelar, "Asymptotic expansions for approximate solutions of boundary integral equations," 2024. [Online]. Available: https://arxiv.org/abs/2411.00060
- [11] W. E. Sherwood, "Fitzhugh-nagumo model," in *Encyclopedia of Computational Neuroscience*, D. Jaeger and R. Jung, Eds. Springer, 2013, pp. 1–11.
- [12] J. R. Delfin, F. Guo, N. Hashimoto, and O. Fujita, "Determination method of markstein number based on wavenumber measurement of cellular flames at the onset of parametric instability of downward propagating flames," *Proceedings of the Combustion Institute*, vol. 40, no. 1-4, p. 105322, 2024. [Online]. Available: https://doi.org/10.1016/j.proci.2024.105322
- [13] M. Al-Khafaji, J. Yang, A. S. Tomlin, H. M. Thompson, G. de Boer, K. Liu, and M. E. Morsy, "Laminar burning velocities and markstein numbers for pure hydrogen and methane/hydrogen/air mixtures at elevated pressures," *Fuel*, vol. 354, p. 129331, 2023. [Online]. Available: https://doi.org/10.1016/j.fuel.2023.129331
- [14] C. Johansen and G. Ciccarelli, "Modeling the initial flame acceleration in an obstructed channel using large eddy simulation," *Journal of Loss Prevention in the Process Industries*, vol. 26, no. 4, pp. 571–585, 2013.
- [15] V. Bychkov, M. Modestov, and M. Marklund, "The darrieus-landau instability in fast deflagration and laser ablation," *Physics of Plasmas*, vol. 15, no. 3, Mar. 2008. [Online]. Available: http://dx.doi.org/10.1063/1.2898402

ACKNOWLEDGMENTS

We extend our deepest gratitude to our advisors, Professors Hongling Cai and Liping Cheng from Nanjing University. Their exceptional guidance was instrumental, providing us with invaluable theoretical insights, expert data analysis, and instruction in academic writing. Their unwavering support and insightful feedback were the bedrock of this research, and their expertise helped us navigate challenges and shape the direction of this study. We are particularly grateful for their patience and understanding during this journey.

Our heartfelt thanks go to our family and friends for their unwavering support. They provided us with a crucial emotional sanctuary during times of exhaustion, and their belief in us was a constant source of motivation. Their companionship and encouragement were essential to our resilience and optimism throughout the research process.

We are truly grateful to the Yau for providing us with this wonderful opportunity. It was through their platform that we were able to unite as a team and tackle this challenge, demonstrating the power of cooperation. This experience accelerated our personal growth while also creating unforgettable memories for us.

Finally, we want to thank our team members for their dedication and perseverance. Each member played an indispensable role, bravely facing difficulties and offering help when needed. Their tireless efforts, including late nights to complete tasks, were fundamental to the success of this project.

This project was inspired by Problem 17 of the 2026 International Young Physicists' Tournament, which tasked us with investigating flame propagation in rings.

AUTHOR CONTRIBUTIONS

Yanting Song (Grade 11): Yanting is a contributor to the project's experimental and analytical phases. Yanting also played a crucial role in visualizing the research by creating diagrams that compared experimental findings with theoretical predictions. His expertise extended to the computational side, where they researched PINN and CFD algorithms, developed mesh strategies, and performed detailed flame velocity analysis. He played a significant role in promoting the intuitive presentation of experimental and theoretical results. Awards:

• AMC 10, Top 5%, 2024

- CMO, Third Prize of Jiangsu Province, 2025
- JSYPT participant (team), Silver, 2025
- The 21st FLTRP CUP National English Competition, Second Prize, 2025
- National English Proficiency Competition for High School Students, Third Prize, 2024

Yiyi Xu (Grade 12): Yiyi is our lead theorist for the team. She developed the theoretical framework for the research and established the isomorphism proof. She was instrumental in investigating the complex relationships between flame velocity and various parameters. Yiyi's contributions also included designing the 3D model for the ring and taking charge of the thesis writing. Awards:

- AMC 12, Top 5%, 2023
- CMO, Third Prize in the competition area, 2024
- CNBO, Second Prize of Jiangsu Province, 2024
- FLTRP Cup, Jiangsu Division First Prize, 2024

Kaiyan Yao (Grade 10): Kaiyan is an essential team member who focused on the experimental validation of the project's models. He was responsible for conducting the experiments and performing precise measurements to validate the accuracy of the team's models. He also took the lead on conducting experiments and was responsible for analyzing the resulting data based on experiments. He takes the experimental conclusions as the basis to assist in studying the influence of parameter changes on the models. Awards:

- MYPT participant (individual), Silver, 2025
- JSYPT participant (team), Silver, 2025
- Chinese National Era Mathematics, First Price, 2024
- 14th CYECC Youth English Proficiency Showcase Nanjing Division, First Prize, 2023

DATA AVAILABILITY

All datasets, codes, and supplementary materials are available at: https://github.com/Xuyiyi3846/traveling-flame-code.git.